PERFORMANCE OF WAVELET DENOISING AND AUTOMATIC DETECTION OF ACTION POTENTIALS ON SIMULATED AND REAL ELECTRNEUROGRAPHIC RECORDINGS

by

MANIKANDAN RAVI

Presented to the Faculty of the Graduate School of

The University of Texas at Arlington in Partial Fulfillment

Of the Requirements

For the Degree of

MASTER OF SCIENCE IN BIOMEDICAL ENGINEERING

THE UNIVERSITY OF TEXAS AT ARLINGTON

May 2013

ACKNOWLEDGEMENTS

This thesis is the product of unconditional support from my professors, friends and family. First and foremost, I would like to thank my guide and mentor Dr. Khosrow Behbehani, for without his initiative, continued guidance and wealth of knowledge, this simply could not have been possible. This research also would not have been possible if not for Dr. Mario Romero-Ortega and I heart fully thank him for providing most of the material necessary for this thesis and giving invaluable ideas throughout the way. I also would like to thank Dr.Georgios Alexandrakis for agreeing to be on my committee and coping with all the date changes patiently.

I would like to thank Vidhi Desai for agreeing to be the expert scorer and spend lots of time during busy semesters to contribute to this thesis. I would also like to thank Sanjay Anand for agreeing to the 'inexperienced' scorer.

I would like to thank my friends both from far and near for putting up with my weird schedule and supporting me all the way. I specially thank Jennifer for being there and keeping me company throughout my thesis. I also would like to thank my research lab partners for all the help that they have given me. Also, I thanks all my colleagues and supervisors at work especially Asha for understanding that I need time to complete my thesis.

Lastly, I simply couldn't have done this if not for a caring brother, a wonderful dad and a lovely mom.

April 19, 2013

ABSTRACT

PERFORMANCE OF WAVELET DENOISING AND AUTOMATIC
DETECTION OF ACTION POTENTIALS ON SIMULATED
AND REAL ELECTRNEUROGRAPHIC
RECORDINGS

Manikandan Ravi, M.S

The University of Texas at Arlington, 2013

Supervising Professor: Khosrow Behbehani

About 1 in 200 people living in the U.S have had an amputation at some stage in their lives. Development of neurally controlled artificial limb prosthesis with the ability to finely control motor activity continues to prove difficult for researchers in the field. One approach is to use the signals obtained from the peripheral nerves by placing an intraneural electrode in the nerve. Since this signal is very noisy, much of the useful information is either lost or buried in the noise even after FIR filtering. Furthermore, there is a need for fast, automated detection of action potentials in order to assess the neural activity in real time.

This study analyzes the performance of wavelet denoising using Discrete Wavelet Transform and Stationary Wavelet Transform against FIR filtering by analyzing noise reduction, detection sensitivity and detection error in simulated electroneurographic (ENG) signals and real ENG recordings. Also, this study compared the sensitivity and detection error between manual detection and automatic detection using template matching technique on Finite Impulse Response filtered as well as Discrete Wavelet Transform denoised ENG signals. Furthermore,

this study also evaluated the effect of choice of wavelet and level of decomposition (parameters of wavelet denoising) on noise reduction, sensitivity of detection and detection error to determine the optimal parameters for wavelet denoising of ENG recordings. From the results of this study, it can be concluded that wavelet denoising of ENG recordings reduce the noise significantly better than Finite Impulse Response (FIR) filtering (p-value = 3.11 E-06). Also, Automatic detection on Stationary Wavelet Transform denoised signals provided optimal sensitivity and detection error than all other detection modes compared. Among all wavelets and levels of decomposition compared in this study, five level decomposition with ‘symlet 7’ wavelet provided optimal noise reduction and sensitivity of detection while also providing significantly lower detection error.

TABLE OF CONTENTS

LIST OF ILLUSTRATIONS

Figure Page

LIST OF TABLES

CHAPTER 1

INTRODUCTION

1.1 Overview

The presence of electrical activity in the body has been known to man for a very long time. Historical records show that in as long back as 340 B.C., Aristotle, when studying behavior of torpedoes (commonly known as 'electric rays'), was the first to notice it. But no serious attempt was made to understand the nature of this effect until Luigi Galvani, Professor of Anatomy at the University of Bologna, Italy in 1787 demonstrated that the muscles in the hind limb of a frog showed electrical properties. He named this type of electricity, "Animal electricity". This study proved to be pivotal in the field of bioelectricity or electrophysiology. The first recording and measurement of electrophysiological signals from living tissues was done by Emil DuBois-Reymond in 1843 using a galvanometer (Burch & DePasquale, 1964).

1.1.1 Neural signal: Detection of Neural activity

Carlo Matteucci first reported the detection of neural activity although he did not assign a specific name to it. Later, DuBois-Reymond in the year 1848 studied it and named the phenomenon, "negative variation", which is known nowadays as "action potential". He improved the galvanometers used during that time to provide more resolution, thereby enabling him to actually record action potentials. He named them "negative variations" because of the fact that during excitation, outer membrane of the nerve became negative with respect to an inactive region. He was also the first to suggest that some chemical process might be the reason of delay of action potential when travelling from nerve ending to the muscle (Piccolino, 1998). Around the same time, in the year 1850, Hermann Von Helmholtz also measured the speed of propagation of the nervous signal, which was considered near impossible by Carlo Matteucci, both Helmholtz's and DuBois-Reymond's mentor. Von Helmholtz built a timing device to

measure the time taken for the stimulated signal to travel from a point in the nerve to another. By knowing the distance between the points and the exact time taken, he measured the conduction velocity as anywhere between 50 – 100 meters per second (Schuetze, 1983). Julius Bernstein, in the year 1868, performed a similar experiment but with a different machine, known as a “differential rheotome” to examine the results for the action potential itself. Much later in 1902, Bernstein proposed based on the works of Nernst, what was at that time, a comprehensive theory of resting and action potentials known now as the membrane theory of excitation (Piccolino, 1998). Using his “differential rheotome”, he was also the first to record the time course of an action current (Figure 1.1).

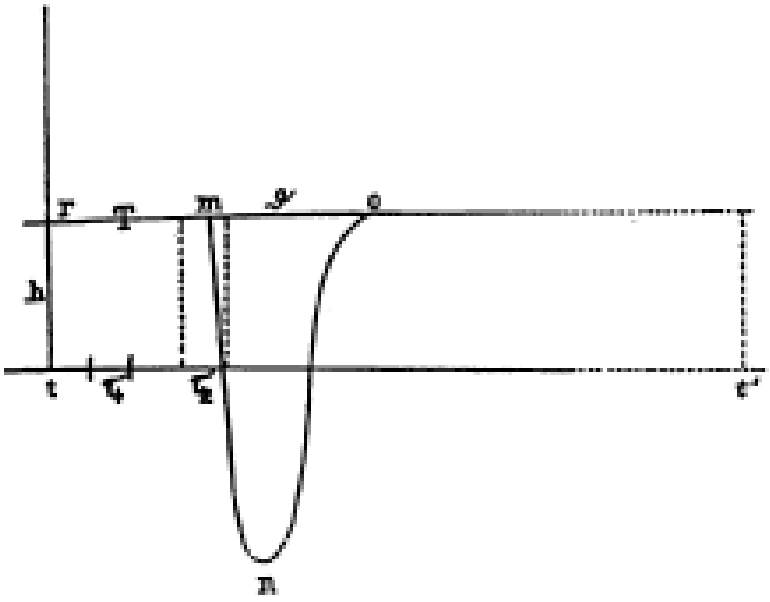

Figure 1.1: First published recording of the time course of an action potential (‘Negative variation”) as published by Julius Bernstein (Bernstein, 1868).

American physiologist H.P. Bowditch in 1871, when studying heart muscle put forward a theory that is known now as the “all or none” law which states that the amplitude of the action potential is constant regardless of the strength of the stimulus that produces it. In 1907, a french neuroscientist named Louis Lapicque postulated that action potentials were generated when the

resting potential exceeds a threshold. In 1949, Alan Hodgkin and Bernard Katz demonstrated the role of sodium ion permeability for an action potential and Hodgkin along with Andrew Huxley postulated a model now known as the Hodgkin-Huxley model of action potential based on the underlying ionic processes and several studies after them, most notably by Erwin Neher and Bert Sakmann concurred with their model while making minor additions (Piccolino, 1998). Most recently, researchers have begun to examine the structural basis for ionic channels using X-Ray crystallography and electron microscopy (Jiang *et al.*, 2003; Sato *et al.*, 2001).

For a neuron at rest, there is a high concentration of sodium and chloride ions in the extracellular fluid than the intracellular fluid, where there is higher concentration of potassium ions. This concentration gradient gives rise to a potential difference known as resting membrane potential of a neuron (usually around -70 mV). When a stimulus exceeds the threshold voltage level (usually around -55 mV), depolarization phase ensues which is characterized by the opening of sodium ion channels which causes sodium ions to cross the cell membrane thereby resulting in increasing the potential (up to +30 mV). After which, repolarization phase occurs when sodium ion channels close and potassium ion channels open thereby causing potassium ions to leave the cell, making the voltage drop close to resting potential. Usually there exists a phase known as hyperpolarization phase where after repolarization, the voltage drops even below resting potential (under shoot) due to continued efflux of potassium ions and following this phase, the neuron goes into a refractory period (about 2 ms) where no action potentials will be generated. After the refractory period, normal ion concentrations are restored by an active process known as the sodium-potassium pump. The current accepted form of action potential is shown in figure 1.2.

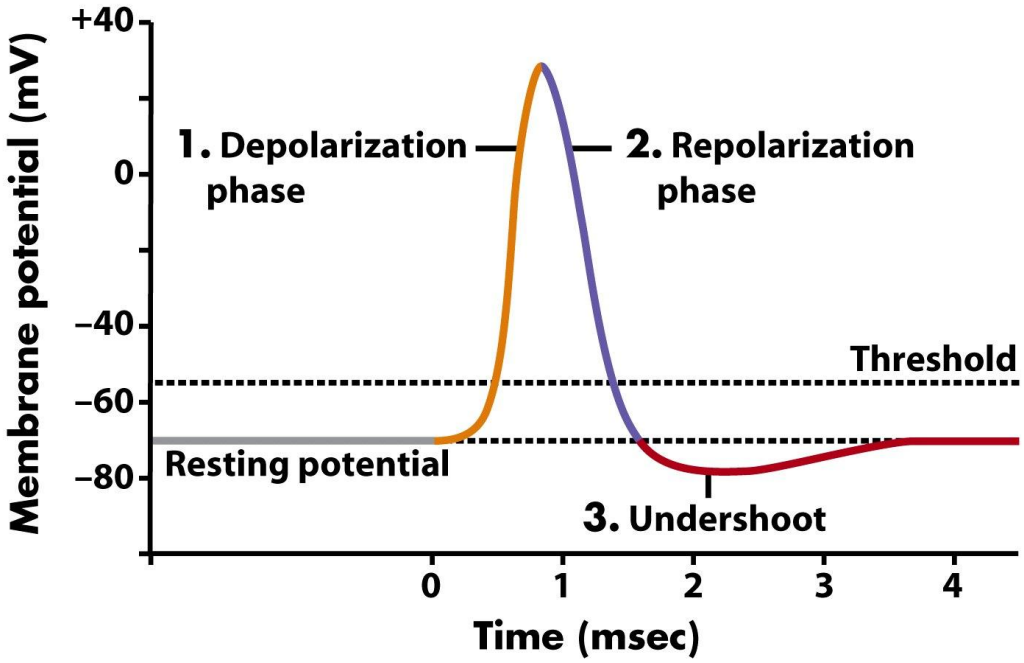

Figure 45-5 Biological Science, 2/e
© 2005 Pearson Prentice Hall, Inc.

Figure 1.2: Shape of an action potential with its various phases marked on it.

1.1.2 Application: Prosthetic Control

One field where ENG is beginning to be used increasingly over the last decade is prosthetic control. There are more than 1.7 million people in the United States alone who have suffered a major limb loss, approximately 1 in 200 persons (Resnik *et al.*, 2012). It has been shown by many studies that subjects who use prosthesis as a result of upper limb amputation are not satisfied with them and many end up abandoning their usage altogether (Biddis & Chau, 2007).

The common reasons for abandonment of upper limb prostheses are phantom limb pain, development of one-handedness as well as constraints in strength, mobility and flexibility (Atkins *et al., 1996*; Dakpa, 1997). It is also shown that among the different types of prostheses, Myoelecric prostheses had the least rejection rate (Biddis & Chau, 2007). Myolectric prostheses are the ones that use electromyography (EMG) for their operation. While EMG is being used as a control signal in prosthetic devices, there are a number of limitations such as the need for

usage of large electrodes, higher number of electrodes, continuously changing properties of muscles because of length changes and fatigue (Stein & Mushahwar, 2005).

The use of ENG signals from Peripheral Nervous System (PNS) can not only overcome the constraints of using EMG but potentially can also be used to provide feedback via the use of bidirectional neural interfaces, thereby restoring physiological conditions to a certain extent (Jia *et al.*, 2007). Moreover, if the information transported via the peripheral nerve can be meaningfully interpreted by a combination of advanced signal processing and artificial intelligence, prosthetic devices with many degrees of freedom can be created and hence, the normal functioning of the limb can be partially restored. As recent research activities by Defense Advances Research Projects Agency (DARPA) and DEKA Research and Development suggest, robotic technology have advanced to such a level that it is now possible to construct fully functioning prosthetics that can be compared with the human arm. But interfacing such prostheses with neural signals and providing biofeedback so as to recover full function of the lost limb still continues to be a formidable challenge.

1.2 Peripheral Nerve Interface

1.2.1 Neural Interfacing

Interfacing with the Nervous System is a crucial part of any device that strives to use neural activity as the input or control signal. Nervous system in our body is divided primarily into two: Central Nervous System (CNS) and Peripheral Nervous System (PNS). Neural Interfaces can be classified largely into three types: Cortical Interfaces, Spinal Cord Interfaces and Peripheral Nerve Interfaces.

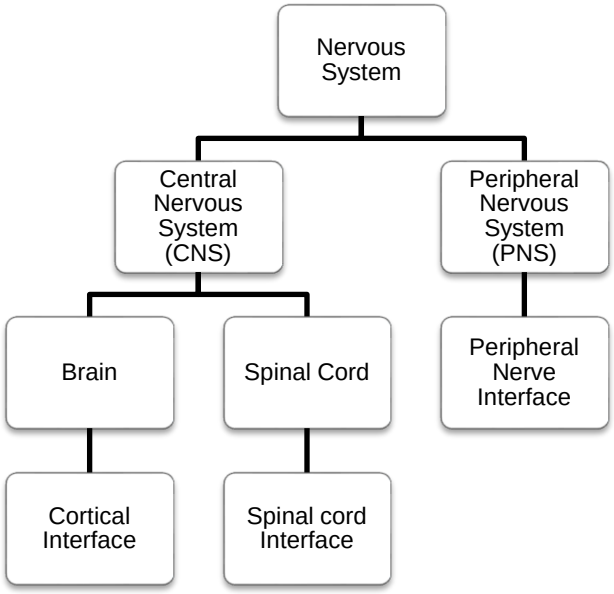

Figure 1.3: Overview of Types of Nerve Interfaces

Cortical Interfaces are the most developed among the three types of Interfaces as most of the research in the area of Neural Interfaces is associated with Cortical Interface. Several studies have shown that control of devices with multiple degrees of freedom can be achieved using cortical interfaces in both primates as well as human subjects (Velliste *et al.*, 2008; O'Doherty *et al.*, 2011). Main drawback with cortical interfaces is that signals from the brain require extensive processing to identify specific outcomes but an even bigger concern is the invasiveness of the interface. While there are less invasive cortical interfaces (e.g. Electroencephalograph (EEG), they lack much of the specificity of a more invasive interface. It is established that the more invasive an interface, the more selective or specific it is and vice versa (Navarro *et al.*, 2005). Moreover, an upper arm amputee might not risk an open brain surgery to gain control of a prosthetic arm. Therefore a peripheral nerve interface could be the most promising option for control of prosthetic devices.

1.2.2 Types of Peripheral Nerve Interface

Peripheral Nerve Interfaces (PNI) can be classified broadly into two categories based on the site of interaction with the nerve itself as Extraneural and Intraneural Interfaces. An

overview of the different types of peripheral nerve interfaces is provided in figure 1.3. It is to be noted that invasiveness and selectivity are considered to be linear parameters in neural interfaces i.e. more invasive interface offers good selectivity and a less invasive interface suffers from poor selectivity. Interfaces are chosen depending on the type of application and necessary selectivity needed. It is also important to note that less selectivity means a proportional increase in sophistication of processing algorithms to extract desired information.

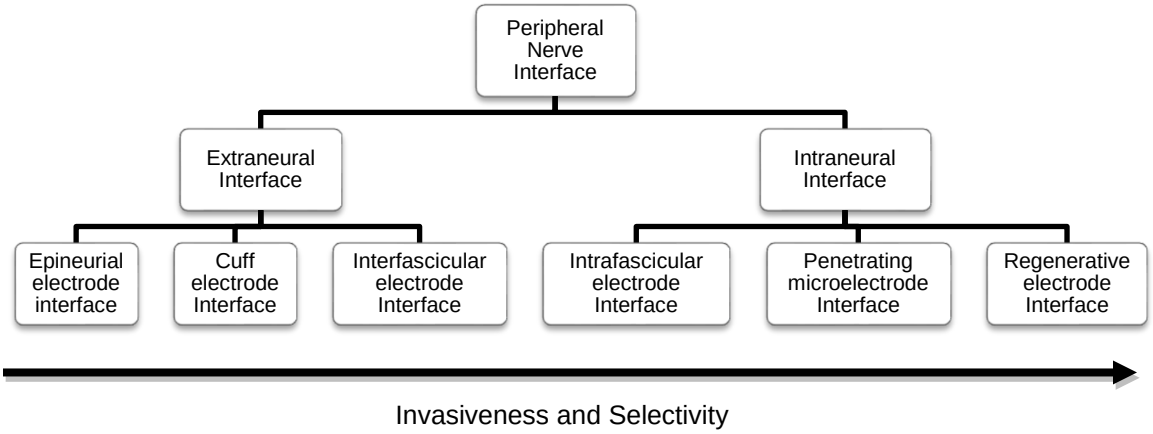

Figure 1.4: Overview of the different types of Peripheral Nerve Interfaces

In figure 1.4, the different types of PNI are arranged from left to right in terms of invasiveness and selectivity. Epineurial electrode interface is the least invasive and least selective of all the Interfaces mentioned, while regenerative electrode Interface is the most invasive as well as the most selective. A brief overview of all the types mentioned above is provided in the following sub-sections while that of Regenerative electrode Interface is provided in the next section.

1.2.2.1 Epineurial Electrode Interface

As the name suggests, epineurial electrodes are electrodes that are planted on top of the nerve and are secured by suturing them to the epineurium of the nerve (figure 1.5 (a)). One of the advantages of this type of interface is that they do not cause much traumatic injury to the nerve itself and any injury caused would only be superficial and will not affect the functioning of

the nerve. However, due to the loose attachment to the nerve, these electrodes show a tendency to disconnect from the nerve when there is excessive motion. This type of electrode is found particularly useful for stimulation purposes such as Functional Electrical Stimulation (FES) and relief of neuropathic pain (Chervin & Guilleminault, 1997; Strege *et al*., 1994).

1.2.2.2 Cuff Electrode Interface

These are composed of an insulated tube that is placed over the nerve, completely encircling it. These typically have three (or more) contacts on their inner surface that are in turn connected to an insulated wire (figure 1.5 (b)). Cuff electrode interface is the type of Peripheral Nerve Interface that has been most researched upon and therefore most prevalent for various applications. There are several advantages in using a cuff electrode such as minimal mechanical distortion, fairly specific stimulation of a particular part of the nerve, comparatively easy surgical procedure (Navarro *et al.*, 2005). Unlike epineurial electrodes, these have been used for detection and stimulation purposes, some electrodes even possessing the capability to do both (Korivi & Ajmera, 2011). However, there are some disadvantages too with the main one being the low signal to noise ratio when compared with other more penetrative electrode interfaces.

1.2.2.3 Interfascicular Electrode Interface

Interfascicular electrode Interfaces combine the simplicity and safety of extraneural interfaces and closer axonal contact of intraneural interfaces. Electrical contacts are placed within the nerve by penetrating the epineurium but outside the fascicle, keeping the perineurium intact. A type of interfascicular interface called the slowly penetrating interfascicular nerve electrode (figure 1.5 (c)) has been used for effective surface activation of peripheral nerves (Tyler & Durand, 1997).

1.2.2.4 Intrafascicular Electrode Interface

Intrafascicular electrodes are placed inside the peripheral nerve and they are in direct contact with the nervous tissue that they are recording or stimulating. This allows for increased

selectivity and improved signal quality than extraneural interfaces (Navarro *et al.*, 2005). A type of intrafascicular electrodes called the longitudinally implanted intrafascicular electrodes (LIFEs) is capable of interfacing with restricted subsets of axons in fasciculated nerves. LIFEs are constructed from thin insulated conducting wires and are implanted longitudinally within the individual nerve fascicles (figure 1.5 (d)).

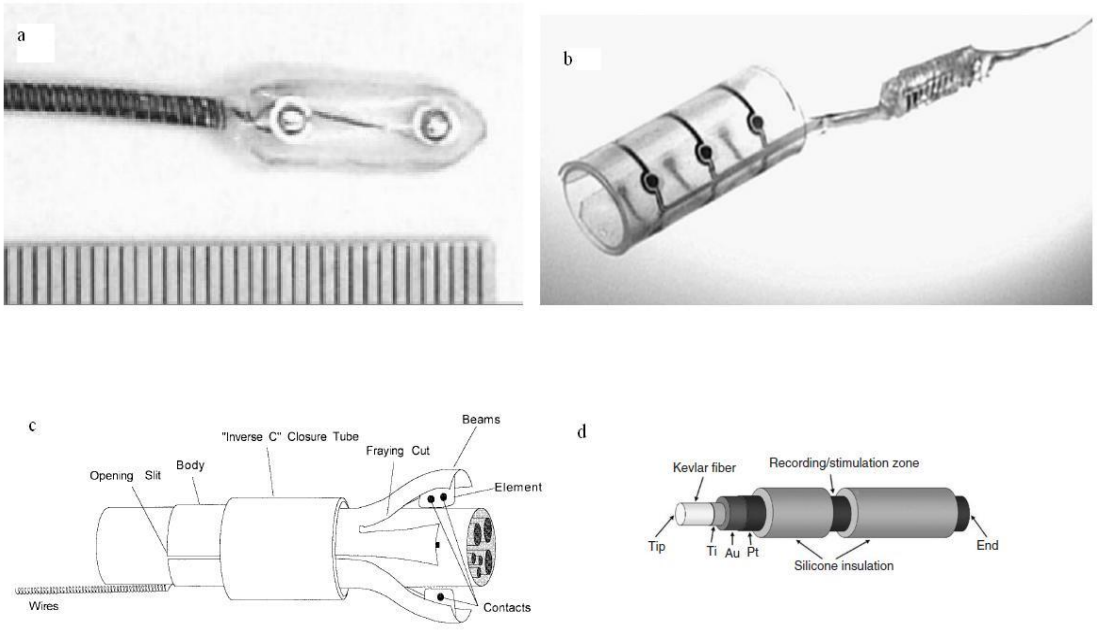

Figure 1.5 (a) Example of an epineurial electrode (Finetech implantable Drop Foot) (b) Example of a cuff electrode (IMBT) (c) slowly penetrating interfascicular nerve electrode (Tyler & Durand, 1997) (d) polymer-based intrafascicular electrode (polyLIFE) (Lawrence *et al.*, 2003). Images adopted from Navarro *et al.*, 2005.

1.2.2.5 Penetrating Microelectrode Interface

The Penetrating microelectrode interface or the microelectrode array (MEA) interface have been used in human subjects for a long time and has proven to be an invaluable tool in examining the physiology and pathophysiology of various peripheral nerves (Hagbarth, 2002). When done with a single electrode instead of an array, this techinique is called as

microneurography and the recordings from the electrodes are called microneurographic recordings or microneurographic nerve activity (Diedrich *et al.*, 2003). with a MEA interface, it is possible to stimulate just a single axon although in most cases, it affects a small bunch of axons (Torebjörk *et al.*, 1987). A research group from University of Utah has designed a microelectrode array (MEA) (called the Utah MEA) with 100 or more electrodes (Figure 1.6) have been developed for use in peripheral nerves (Branner & Normann, 2000). A variation of this electrode with a slanted array of electrodes with their length varying from 0.5 to 1.5 mm has also been developed (Branner *et al*., 2001). They have shown that the electrodes in the array were capable of recording single-unit action potentials from axons in response to stimuli and capable of controlling a robotic limb with one degree of freedom (Navarro *et al.*, 2005)

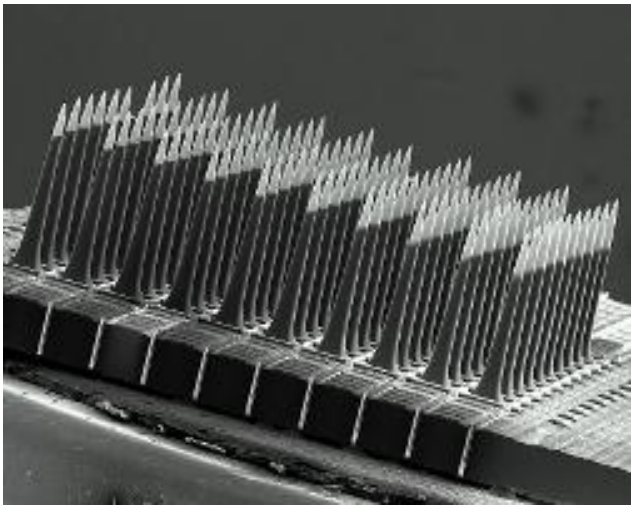

Figure 1.6: A picture of a type of Penetrating microelectrode interface designed by researchers from University of Utah (Image adopted from Microsystems lab, University of Utah)

1.2.3 Regenerative Electrode Interface

Regenerative electrodes are implanted between the severed stumps of a peripheral nerve and due to its regenerative properties, eventually grows back through the electrode interface. This type of electrode interface is one of the most selective as well as being the most invasive interface among all the interfaces mentioned (Kovaks *et al.*, 1992). However,

the success of this type of interface relies on the success of regeneration of the axons through the perforations in the electrode and the biocompatibility of the material used in the electrode itself (Navarro *et al.*, 1996). First published recordings from a regenerative electrode were made in 1974 by Mannard *et al.* and are shown in figure 1.7. The recordings were taken from the sciatic nerve of a frog. At first silicon sieve electrodes were used predominantly to demonstrate regeneration of axons and to record neural activity from peripheral nerves of rats and frogs (Navarro *et al.*, 1996; Della Santina *et al.*, 1997). But more adaptive, flexible and stable polyimide-based electrodes began to be used later on (Navarro *et al.*, 1998). More recently, researchers have begun to use a guidance tube or channel to guide and provide a clear path for axonal regeneration (Cho *et al.*, 2008) and another type of regenerative electrode interface proposed by Garde *et al.* uses a needle electrode array inserted into a hollow collagen-filled tube (Figure 1.8) (Garde *et al.*, 2009; Siefert *et al.*, 2012). They have shown that such a non-obstructive regenerative electrode interface is capable of providing early and relatively stable neurointerfacing in peripheral nerves(Garde *et al.*, 2009). This design is known as Regenerative Multi-electrode Interface (REMI) and is used in the experiments that comprise this thesis.

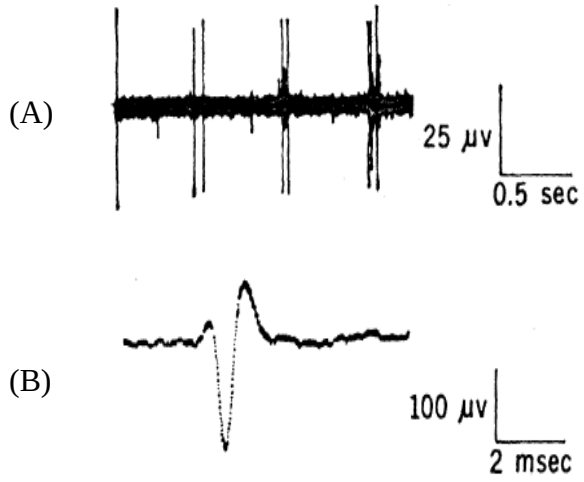

Figure 1.7: First published recordings by Mannard *et al.* using a regenerative electrode interface on the sciatic nerve of a frog. (A) Spike train obtained from a motor nerve fiber while the animal was swimming. (B) A single unit action potential in response to a muscle stretch.
(from Mannard *et al.*, 1974).

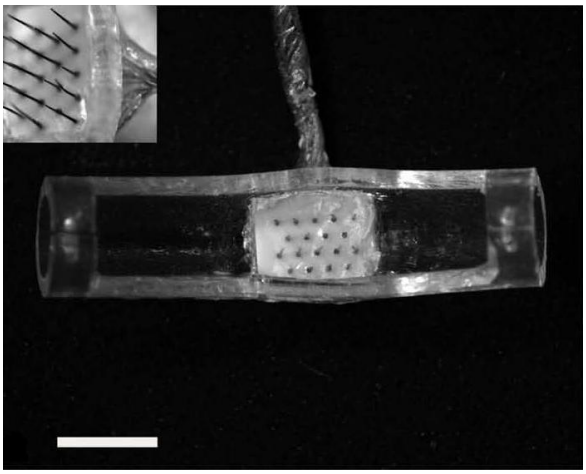

Figure 1.8: The regenerative multi-electrode interface proposed by Garde *et al.*
(From Garde *et al.*, 2009)

1.3 Spike Detection

Detection of action potentials from ENG signal is termed as spike detection. Spike detection is often the first step in quantifying neural activity in the nerve. It is also to be noted that in less invasive interfaces such as the epineurial or the cuff electrode interface, it is sometimes not possible to detect spikes; therefore increase in amplitude of ENG over a period of time is taken as a reflection of neural activity in the nerve.

1.3.1 Overview of Spike Detection

Although there are many ways to perform spike detection, most of them follow the general steps that are shown in figure 1.9. Hardware filtering usually involves a band pass filter and a notch filter that excludes power line interference (50 Hz or 60 Hz). Usually hardware filters are incorporated into the recording system and used primarily to remove very low frequencies and power-line interference. Software filtering is preferred for other purposes because the cut-off frequency used can be varied according to the type of recording. Software filtering involves either an additional filter specific for the application although of late, wavelet denoising (explained in detail in chapter 2) has been used extensively in addition to a band pass filter in ENG applications (Citi *et al.*, 2008). A Thresholding algorithm is used to detect spikes or to extract possible spikes that are later processed by a detection algorithm to determine

whether they are real spikes or not. It involves setting a preset or varying value and the waveforms that cross this value (threshold) are extracted for further processing. Sometimes, manual detection is also used to determine and classify spikes.

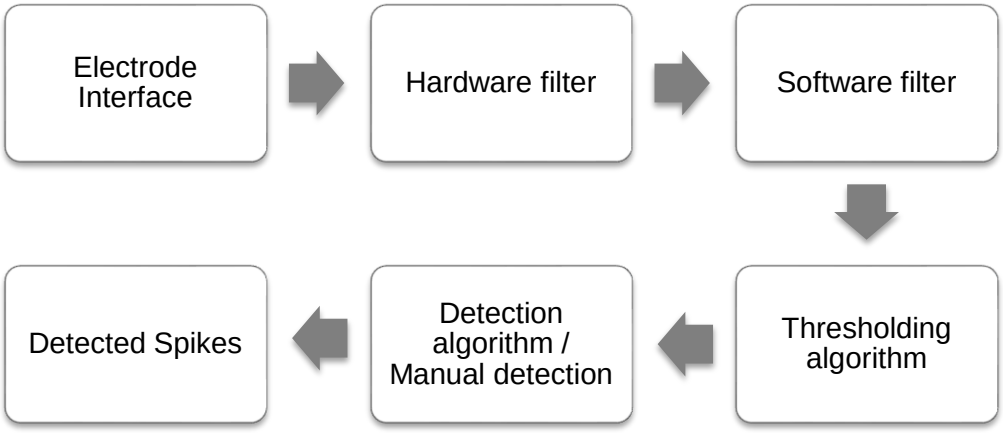

Figure 1.9: Overview of general steps involved spike detection

1.3.2 Current Methods

Major differences in the methods used for spike detection is in software filtering, thresholding and detection steps. Different methods used for each of those steps are briefly reviewed in the following subsections.

1.3.2.1 Methods used for Software Filtering

ENG signals are generally very noisy signals which necessitate extensive filtering in order to effectively filter out the noise in the waveform. In addition to any hardware filters, usually a band pass filter whose lower cut-off frequency can range from 300 – 800 Hz and whose higher cut-off frequency can range from 2 – 6 KHz (Diedrich *et al.*, 2003; Brychta *et al.*, 2007; Zhang *et al.*, 2007; Wiltschko *et al.*, 2008; Seifert *et al.*, 2012). However even after software filtering using the band pass filter as specified, noise in the signal remains high and much of the useful information (in this case, action potentials) can still go undetected when thresholding is applied. A new method of denoising called wavelet denoising was implemented

on ENG signals by Oweiss and Anderson in 2002 and a variation of it by Diedrich *et al.* in 2003 (Oweiss & Anderson, 2002; Diedrich *et al.*, 2003). It is based on wavelet transform (Mallat, 1989; Daubechies, 1990) and a detailed explanation is provided in chapter 2. Many researchers have implemented the wavelet denoising step in their filtering process and results show that this enhances the SNR better than just band pass filtering (Diedrich *et al.*, 2003; Citi *et al.*, 2008).

1.3.2.2 Methods used for Thresholding

Most common method used for thresholding the ENG signals is the simple one way thresholding where all the spikes that cross a set threshold value (that is set manually or calculated based on the standard deviation of the signal) in either the positive direction ("positive threshold') or in the negative direction ("negative threshold") are extracted for further processing (Diedrich *et al.*, 2003; Brychta *et al.*, 2008; Vargas-Irwin & Donoghue, 2007; Zhang *et al.*, 2007; Citi *et al.*, 2008). Some studies use more elaborate algorithms such as the nonlinear energy operator (NEO) which considers spikes as sudden increase in both amplitude and frequency and sets the threshold based on the instantaneous energy of spikes (Kim & Kim, 2000; Choi *et al.*, 2006).

1.3.2.3 Detection Methods

Although a lot of automated methods for detection and classification of spikes from ENG signals exist, many studies still use manual detection and classification (Wiltschko *et al.*, 2008; Seifert *et al.*, 2012). The most common method in automatic detection algorithms is the use of principal component analysis (PCA) (Zhang *et al.*, 2004; Choi *et al.*, 2006; Vargas-Irwin & Donoghue, 2007; Adamos *et al.*, 2008). Other methods such as wavelet packet decomposition (Oweiss & Anderson, 2002; Hulata *et al.*, 2002) and using support vector machines (SVMs) (Volgstein *et al.*, 2004) have also been reported. The use of PCA and SVM methods mainly involve extracting variables from the shape of an action potential such as spike width, zero crossing, total amplitude etc. and are clustered. From these clusters, by using a discrimination method (such as Expectation Maximization (EM)), action potentials are isolated. However

clustering can be a time consuming process and real time applications might require reduction of dimensions in feature space for effective spike detection (Thakur *et al.*, 2007).

1.4 Objective and Organization of the thesis

1.4.1 Objective of the study

The overall objective of the study is to implement an effective wavelet denoising algorithm in ENG signals and subsequently to develop a fast and robust method for automatic detection of action potentials. To obtain this overall objective three specific objectives are put forward:

1. Determine the efficacy of various wavelets and levels of decomposition (Parameters of wavelet denoising) suggested from literature.
2. Develop a wavelet denoising algorithm using the best parameters determined and examine its performance on ENG signals and compare with FIR filtering.
3. Develop a fast and robust detection method to automatically detect action potentials from denoised ENG signals and compare its performance against that of manual detection.

To obtain the above specified objectives, the study was divided into two parts. The First part involved the analysis of simulated ENG signals and second part involved the analysis of performance on real ENG signals obtained from a regenerative multielectrode interface (REMI) implanted in the sciatic nerve of a rat.

By implementing an effective denoising technique for ENG signals, long term goals such as monitoring the integrity of the signals obtained from the electrode interface, effective comparison between various electrode interfaces, improving the longevity of electrode interfaces and monitoring effect of changes caused due to growth of nerve surrounding the electrodes in a regenerative electrode interface could be achieved. Also, by implementing an automated detection technique, the ultimate goal of real time implementation for prosthetics could be achieved.

1.4.2 Organization of this thesis

Chapter two of this thesis includes the description of the experimental set up, data collection as well as description of the wavelet denoising algorithm and the detection algorithm used throughout the study. Chapter three presents the results obtained from implementing the algorithms on both simulated and real ENG signals as well as the effect of various parameters on the outcome of the denoised signal. Interpretation and significance of the results in chapter three are elucidated in chapter four along with the limitations of this study and recommendations for future works in this area of study.

CHAPTER 2

MATERIALS AND METHODS

2.1 Electrode Interface

2.1.1 REMI Electrode

Regenerative multi-electrode interface (REMI) (see section 1.2.3 for more details) type of peripheral nerve interface manufactured by Microprobes Inc. (Gaithersburg, MD) was implanted in sciatic nerve of rats. It consisted of 18-pin insulated platinum/iridium electrode array placed in a 5-4-5-4 order with each electrode separated from the other by a distance of 400 µm. Each electrode measured about 50 µm in diameter and the height varied from 0.7 to 1.0 mm. This electrode array was placed inside a 5mm long, 3 mm diameter polyurethane nerve guide tube (Braintree Scientific Inc., Braintree, MA). 4.5 cm long gold wires that were wound in a helix and insulated with Parylene-C formed a cable that connected the REMI electrode array to a connector (Omnetics, Minneapolis, MN). The connector is housed in a titanium pedestal which had flanges to help adhere itself to the pelvic bone. The whole assembly was sterilized prior to surgical implantation by exposure to UV light and the nerve guide tube was filled with 0.3 % liquid collagen (Chemicon, Temecula, CA). For more information on the entire assembly, refer Seifert *et al.*, 2012.

2.1.2 Surgical Implantation

Electrode interface was implanted in the left sciatic nerve of rats, which were anesthetized using inhaled isoflurane mixed oxygen (5% concentration for induction and a 2 – 2.5% concentration was used to maintain the animal in that state). After the animal was anesthetized, dorsal pelvic and leg area was shaved and cleaned with povidone-iodine. An incision was made along the sciatic vein between the semitendinosus and biceps muscles, thereby exposing the proximal part of the nerve. The nerve was transcected and the REMI,

housed in the nerve guide tube was introduced between the nerve stumps. The connector which is connected to the REMI array by gold wires and is housed in a titanium pedestal was mounted on the pelvic bone with bone cement (Biomet Inc., Warsaw, IN). The Skin was sutured along the pedestal with the help of surgical staples. All procedures were performed according to the guidelines of the Institutional Animal Care and Use Committee of the University of Texas at Arlington. For a more detailed description of the surgical procedure, refer Seifert *et al.*, 2012.

2.1.3 Experimental Setup

The titanium pedestal can be connected to a headstage which also serves as a preamplifier. The headstage is connected to the pedestal only during the recording. The headstage is connected to a recording system which is in turn connected to a computer. Cable, headstage, recording hardware and software were all products of Plexon Inc. (Dallas, TX) and were purchased from them. A diagram depicting the full setup is shown in figure 2.1.

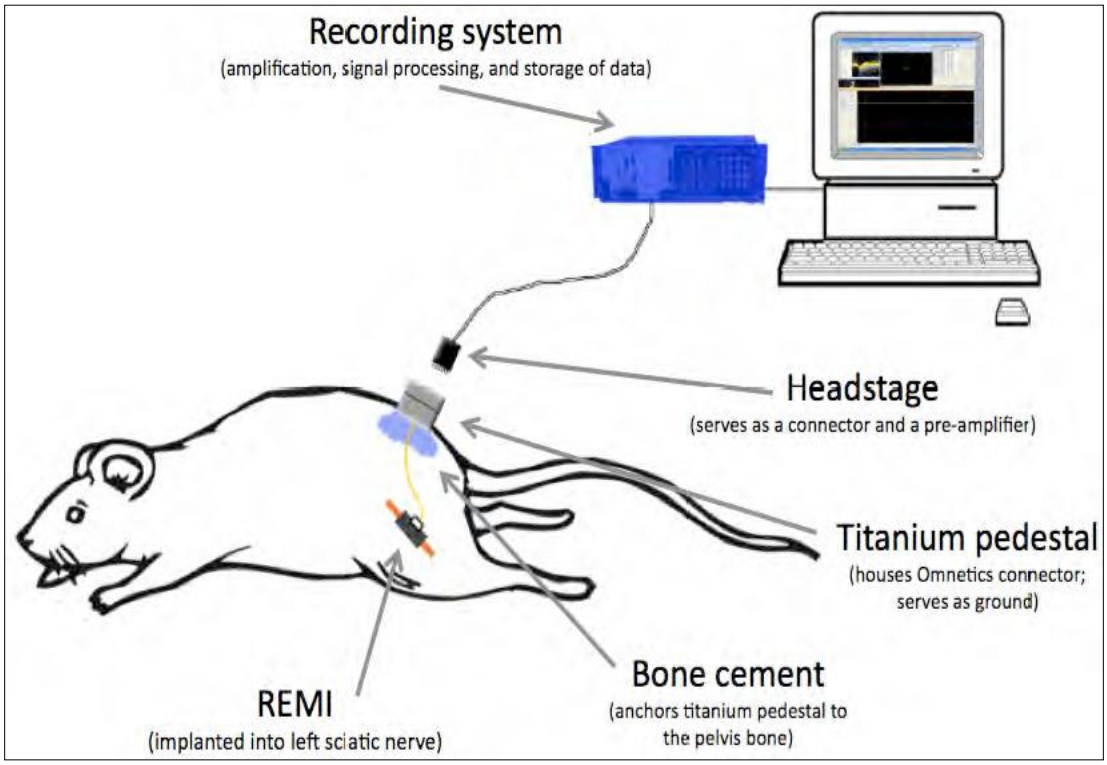

Figure 2.1: Diagram of the experimental setup (From Seifert *et al.*, 2012)

2.1.4 ENG Recording

ENG recordings from each animal were obtained weekly starting at day 7 after implantation. During a recording session, the animal is anesthetized for a brief period of time and the headstage is connected to the pedestal. After the animal has regained consciousness, ENG signals are recorded and a typical recording session lasts about 5 minutes. The signals were recorded from 16 electrode channels at a sampling frequency of 40 KHz. The recording system utilizes a hardware high pass filter with a cut-off frequency of 3 Hz. The animal was anesthetized before disconnecting the pedestal and the headstage after the recording.

2.2 Manual Detection

2.2.1 Software used for Manual Detection

For manual detection of action potentials from ENG recordings, software called Offline Sorter (Plexon Inc., Dallas, TX) was used. In certain cases such as in the analysis of simulated signals for the purposes of this thesis, files of the format "*.nex", belonging to NeuroExplorer (Nex Technologies, Westford, MA) were also analyzed using Offline Sorter. A snapshot of the software is shown in figure 2.2.

2.2.2 Visual Detection of Action potentials

Offline Sorter software has a selection of built-in FIR filters that the score uses to remove the noise from ENG recordings. A threshold value is chosen by the visual judgment of the scorer and the waves that exceed the threshold are shown in the "waveform" window from which the scorer selects the waveforms that classifies as action potentials. A snapshot of the filters and threshold section of the software is shown in figure 2.3. There are tools in the waveform window that allows the scorer to select or deselect waveforms shown in them. The scorer can also classify them into different groups or units. A snapshot of the waveform window is shown in figure 2.4. Although the scorers used the same software for scoring, the exact method varied from scorer to scorer.

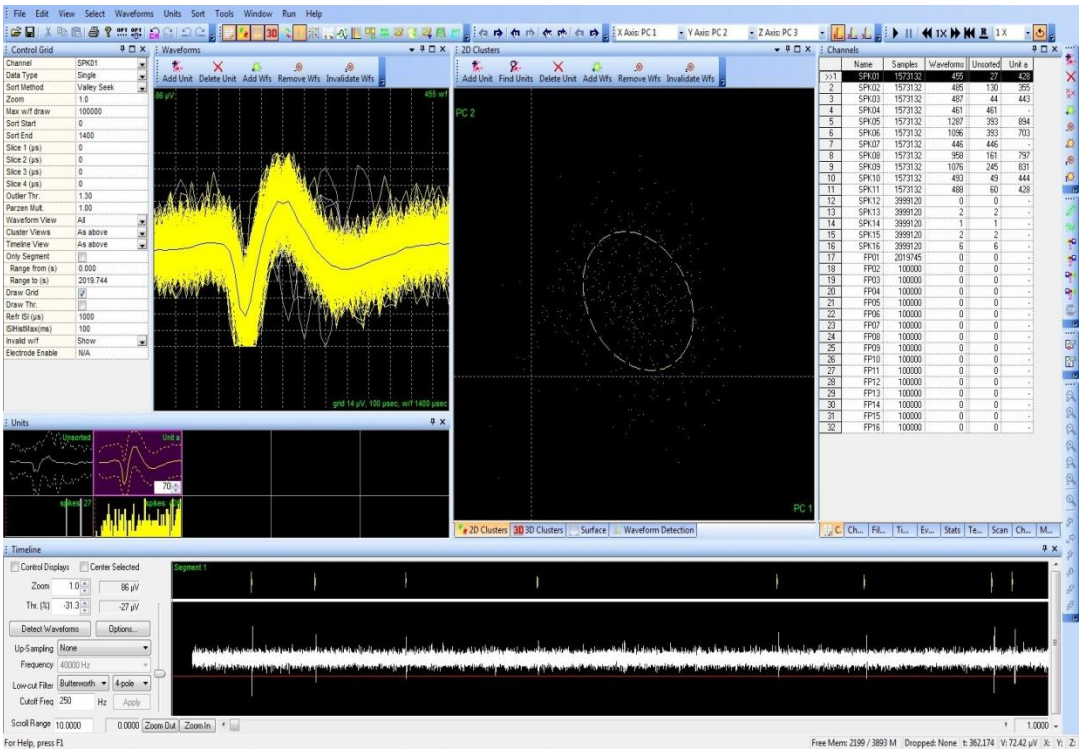

Figure 2.2: Snapshot of Offline Sorter (Plexon Inc., Dallas, TX)

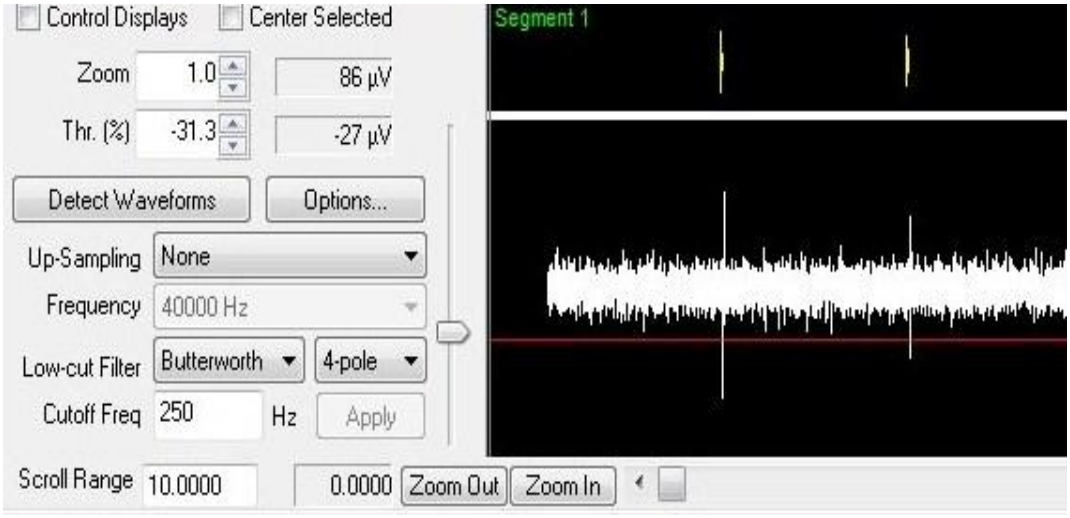

Figure 2.3: Snapshot of the filtering and thresholding section of Offline Sorter software

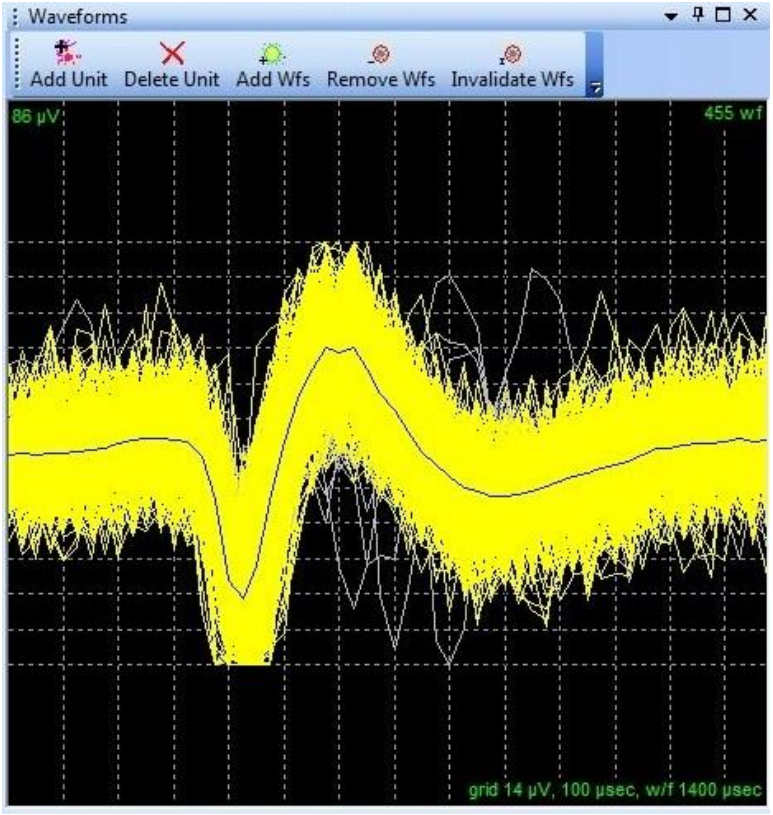

Figure 2.4: Snap shot of the waveform window of the offline sorter software

2.3 Simulated ENG Signal Construction

2.3.1 Action Potentials used in the Simulated ENG Signal

For comparing the different denoising and detection methods, it was essential to use simulated signals because of the prior knowledge of location of action potentials. The simulated ENG signals were generated and analyzed using MATLAB (Mathworks Inc., Natick, MA). The action potentials were obtained from the scores of a trained scorer. A total of about 2500 action potentials obtained from scores of 3 separate ENG recordings constituted the main set from which action potentials were chosen in a random manner to form different simulated signals. The mean of all the waveforms in the set was plotted and is shown in figure 2.5. To test the denoising and detection algorithms in the presence of noise at various levels and to determine

their performances in detecting not only the big, obvious action potentials but also small ones that are closer to the noise baseline, 3 different sizes or “types” of action potentials were used in the construction of the action potential. Type 1 action potentials were the actual size; Type 2 action potentials were two-thirds of the actual size and Type 3 were one-thirds of the actual size.

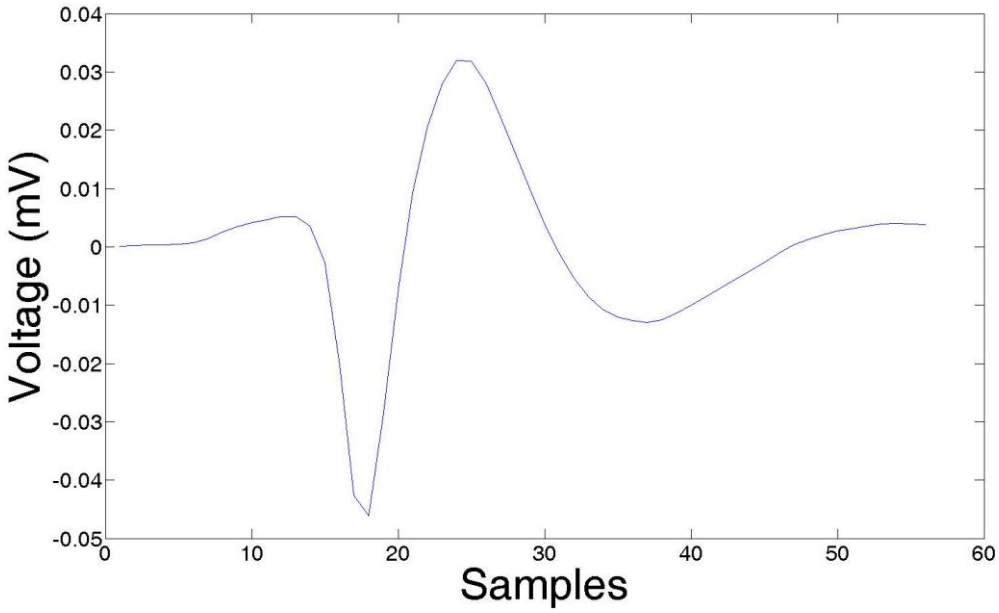

Figure 2.5: Mean waveform of the action potential set

2.3.2 Artificial Noise

In the literature, it is established that the noise present in ENG recordings can be classified as Gaussian (Diedrich *et al.*, 2003; Kamavuako *et al.*, 2010). Hence, MATLAB’s in-built “Add White Gaussian Noise (awgn)” function was utilized to add noise to the simulated signal. Noise was added at five different levels; hence five simulated ENG signals were generated. The levels were chosen in such a way to mimic conditions raging from normal to extreme. The signal to noise ratio (SNR) was measured in all 5 signals and they are displayed in table 2.1. Simulated signals were also visually compared with real ENG recordings by the experienced scorer and were determined to be similar.

Table 2.1: Signal to Noise Ratios (SNRs) of the simulated ENG signals

Simulated Signal	Signal to Noise Ratio (SNR)
Signal 1	10 dB
Signal 2	7.5 dB
Signal 3	5 dB
Signal 4	2.5 dB
Signal 5	0 dB

2.3.3 Generation of Simulated ENG Signal

The total number of action potentials in each signal varied in a random manner and had all 3 types of action potentials in equal amounts. Sampling rate was chosen at 40 KHz, same as the real ENG recordings. Average length was 45 seconds and average number of action potentials present was 792 per signal, with 264 action potentials of each type. The temporal distance between two action potentials (Inter-spike interval) was also chosen in random and ranged from 2.5 ms to 1 s. A segment of simulated signal before adding noise to it is shown in figure 2.6. Then, using built-in MATLAB function (awgn), noise is added according to the SNR specified in table 2.1. Figure 2.7 depicts the same signal in figure 2.6 but after adding Gaussian noise. It is important to note that all 5 signals are in essence, different signals and not different noise levels of the same signal. This was done to ensure that the manual scores of all 5 signals are independent from each other. Table 2.2 lists the number of action potentials of each type, in total and the length of all the simulated signals.

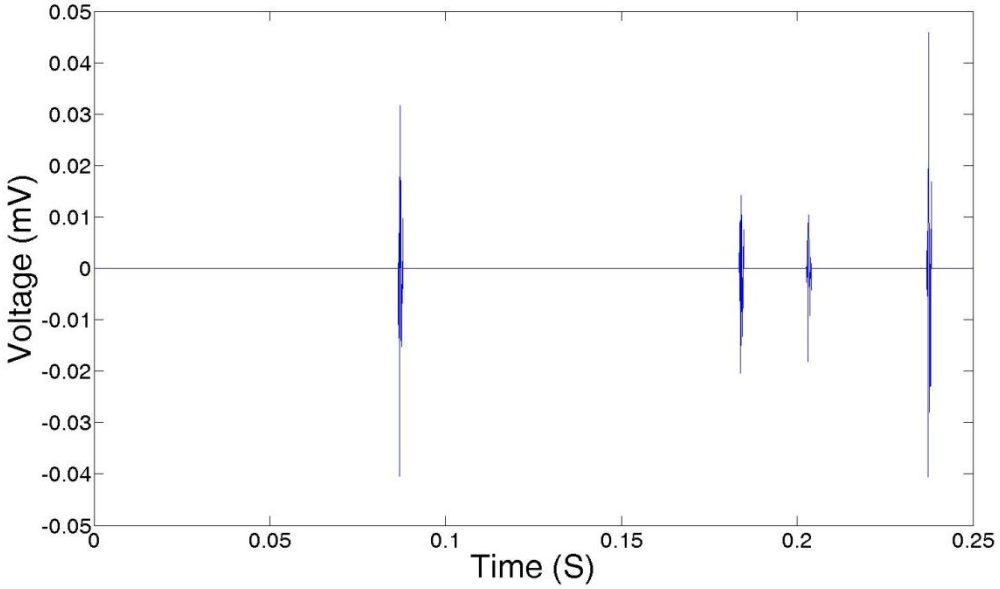

Figure 2.6: Segment of a simulated signal before adding white Gaussian noise

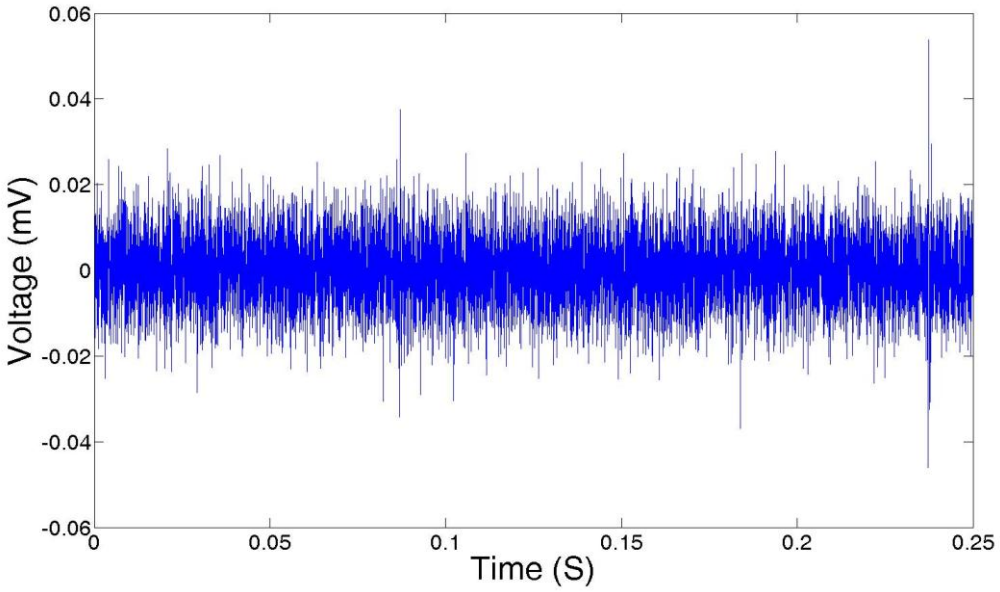

Figure 2.7: Segment of the simulated signal after adding white Gaussian noise (SNR = 5dB)

Table 2.2: Number of action potentials present and length of simulated ENG signals

Simulated signal	Total number of action potentials	Number of action potentials of each type	Length of the signal (in seconds)
Signal 1	795	265	45.48 s
Signal 2	699	233	39.33 s
Signal 3	873	291	48.93 s
Signal 4	768	256	44.73 s
Signal 5	825	275	46.70 s

2.4 Wavelet Denoising

2.4.1 Discrete Wavelet Transform

2.4.1.1 Background

Wavelet transform provides the time-frequency representation of a signal, instead of just frequency representation that Fourier transform provides. Fourier transformed signals do not provide the time localization of different frequencies observed and hence, it is not suitable for analysis of nonstationary signals. Action potentials - obtained from electroneurogram (ENG) - are nonstationary and contain short-lived, high frequency components that are temporally close.

Short Time Fourier Transform (STFT) provides time-frequency localization, but when compared to the wavelet transform, it is not as effective in providing good resolution over both time and frequency domains simultaneously (Akay & Mello, 1997). STFT fails because it uses a constant window length therefore the time and frequency resolutions are fixed, making it difficult to have both good time resolution at higher frequencies and good frequency resolution at low frequencies.

Discrete Wavelet Transform (DWT) overcomes this issue. A simple figure explaining the working of DWT is shown in figure 2.8. DWT involves processing the signal through a series of

high pass filters to analyze the higher frequencies and a series of low pass filters to analyze the low frequencies. At each level, the high-pass and low-pass filters are complementary and have a cut-off frequency of π/2 radians. The coefficients that pass through the low pass filter are called approximation coefficients (denoted by 'A1', 'A2' and so on) and the coefficients that pass through the high pass filter are called the detail coefficients (denoted by 'D1', 'D2' and so on). In DWT, after each level, the coefficients are decimated or down sampled by a factor of two. This process continues until a preselected level, known as level of decomposition. The detail coefficients are then passed through a thresholding algorithm (explained in the next section) and the new coefficients are used to regenerate the signal by using Inverse Discrete Wavelet Transform (IDWT). The whole process is termed Wavelet Denoising.

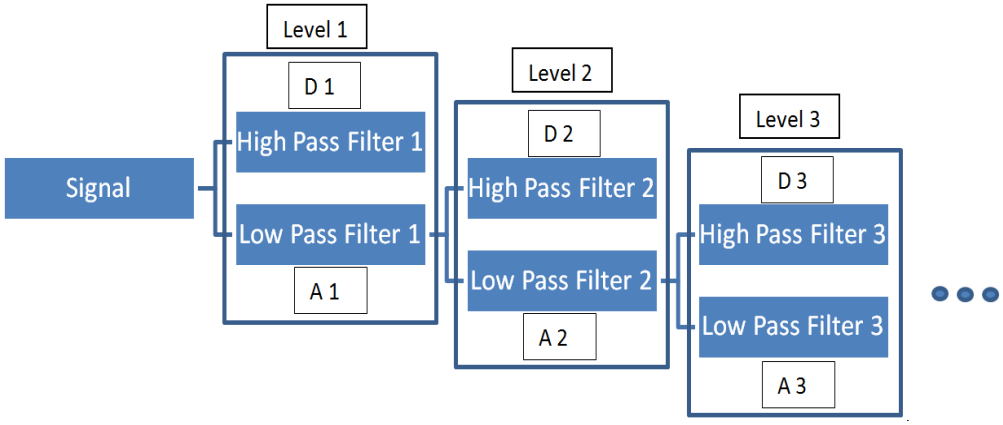

Figure 2.8: Working of Discrete Wavelet Transform (DWT)

2.4.2.2 Thresholding of Detail Coefficients

The correct thresholding of detail coefficients forms the essence of denoising process and therefore after careful considerations and extensive literature review on the topic, a single-level noise estimation threshold was chosen since it performed better than level dependent threshold (Brychta *et al.*, 2007). Hard thresholding was preferred over soft and firm thresholding techniques (Diedrich *et al.*, 2003). The threshold value was selected, as proposed by Donoho, as,

$$T = \sigma\sqrt{\ln(N)}$$

where, σ denotes the standard deviation of the gaussian noise and N denotes the number of samples in the signal. Single level noise estimation threshold means that the same value of T is used across all levels of decomposition for thresholding (Donoho, 1995)

2.4.2.3 Implementation

Both DWT and IDWT were implemented using the functions available in the wavelet toolbox of MATLAB. Two levels of decomposition was chosen for comparison, levels 4 and 5, as these levels of decomposition were found to perform better than other levels (Brychta *et al.*, 2007). In simulated signals, the following wavelets were used: Symlet 7 ('sym7'), Daubechies 4 ('db4)', Haar ('haar'), Biorthogonal 3.5 and 3.7 ('bior 3.5' and 'bior 3.7' respectively). These wavelets were used to compare and find which level of decomposition and which wavelet produces better results and that combination was used to denoise real ENG recordings. A suite of MATLAB-based programs were developed to implement wavelet denoising. The codes for the programs are presented in the appendix section of this thesis.

2.4.2 Stationary Wavelet Transform

2.4.2.1 Differences between SWT and DWT

Stationary Wavelet Transform (SWT) or the Translation-invariant wavelet transform is similar to DWT but differs in the subject of decimating the coefficients. SWT does not decimate the coefficients by a factor of 2 as the DWT does, thereby making it translation invariant. The DWT on the other hand, is translation variant because it decimates or down-samples the coefficients. This makes the SWT more computationally complex, because of the increased number of coefficients at higher levels thereby increasing the processing time.

2.4.2.2 Thresholding of Detail Coefficients

For SWT, a type of thresholding known as the minimax threshold method was used as suggested by Citi *et al.* in 2008, the value of threshold is determined by the formula,

$$T = \sigma(0.3936 + 0.1829log_2(N))$$

where σ denotes the standard deviation of the Gaussian noise and N denotes the number of samples in the signal. This type of thresholding is a more conservative approach and would be more suitable in SWT cases (Citi *et al.*, 2008). For SWT, single level and hard thresholding were applied, same as DWT.

2.4.2.3 Implementation

Both SWT and Inverse Stationary Wavelet Transform (ISWT) were implemented using the wavelet toolbox in MATLAB. In simulated signals two different levels of decomposition and five different wavelets were employed, the details of which are same as the ones used in DWT and are provided in section 2.4.2.3. For both simulated and real ENG signals, denoising was carried out using custom made MATLAB-based programs. The codes developed are given in the appendix section of this thesis.

2.5 Automatic Detection

2.5.1 Overview

The automatic detection of action potentials was carried out in two steps. The first step involved thresholding of the signal to extract candidates for action potentials and this step is explained in detail in section 2.5.2. The second step involved processing these candidate action potentials by a template matching algorithm which determined which of these candidate action potentials could be classified as action potentials and which of those to neglect. Details of the template matching step are provided in section 2.5.3. The detected action potentials are the output of the template matching process and these are then stored along with their actual timestamps. The timestamps are stored for comparison purposes either with scores from manual detection or with actual timestamps of simulated signals which are also stored while generating them. A custom program using MATLAB environment was developed for automatic detection of action potentials.

2.5.2 Preliminary Identification of Action Potentials using the Thresholding Algorithm

A conservative threshold was chosen since a validation procedure in template matching was to follow after this step. Also, a noise dependent threshold was chosen as opposed to manually selecting a value of threshold. Thresholding of candidate action potentials was performed in two steps. First step was to set an initial threshold according to the formula,

$$initial\_threshold = -2 * \sigma$$

where σ denotes the standard deviation of the signal. This is visually shown in figure 2.9. Negative threshold was chosen because the standard action potential has higher amplitude in the negative direction than in the positive direction. All the waveforms crossing this threshold were passed through another amplitude threshold which is calculated as,

$$amplitude\_threshold = 2 * |initial\_threshold|$$

This amplitude threshold is visually shown in figure 2.10. The waveform has to have total amplitude greater than *amplitude threshold* to be saved as a candidate action potential which is then processed by a template matching algorithm.

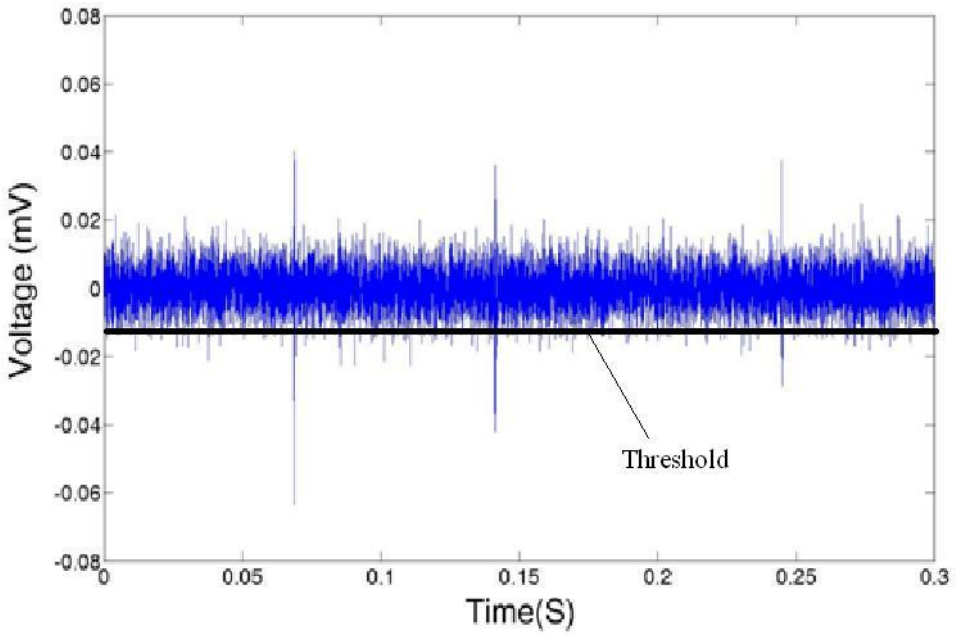

Figure 2.9: Initial thresholding of signal

Theoretically, total threshold can be expressed as,

$$total\ threshold = 4 * \sigma$$

Such a threshold is considered conservative for wavelet denoised signals because the noise is significantly less than that of FIR filtered signals whereas for FIR filtered signals, a threshold of 3 times the standard deviation is considered optimal (Wiltschko *et al*, 2008). If a waveform crosses the initial threshold at point x, then the samples from (x-15) to (x+40) are extracted for further analysis (56 data points in total). In figure 2.10, the two lines in the middle visually depict the amplitude threshold which has to be crossed by a waveform to be classified as a candidate action potential. In the case shown in the figure, the amplitude of the waveform shown exceeds the threshold and therefore it would be stored as a candidate action potential for further analysis by a template matching algorithm.

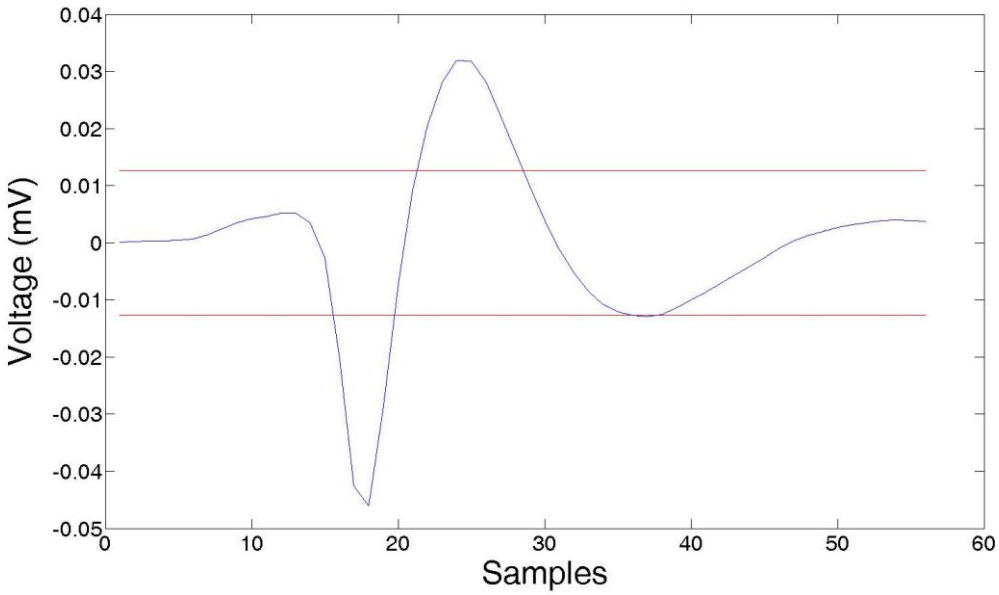

Figure 2.10: Amplitude thresholding of waveform

To validate the thresholding algorithm, 5 simulated signals that are different from the ones used for testing but constructed using the same program were passed through template

matching algorithm before adding noise to them and in all 5 cases, all the waveforms were detected successfully.

2.5.3 Template Matching

Template matching procedure involves matching the candidate action potential with an action potential template that is predetermined. The template was chosen to be the mean waveform of the action potential set (figure 2.5). This was implemented in two steps, the first step was aligning the waveform with the template and the second was to estimate the degree of match with the template.

For aligning the waveform, cross-correlation was performed between the waveform and the template. Then the waveform was aligned according to the lag which corresponded to the maximum correlation value. Next, Pearson correlation coefficient was determined for the aligned waveform and the template. If X is the template and Y is the aligned waveform and n is the number of samples in both (56, in this case), then the pearson correlation coefficient can be calculated as,

$$R = \frac{\sum_n (X_n - \overline{X})(Y_n - \overline{Y})}{\sqrt{\left(\sum_n (X_n - \overline{X})^2\right)\left(\sum_n (Y_n - \overline{Y})^2\right)}}$$

where $\overline{X}$ and $\overline{Y}$ represent mean value of X and Y respectively. The candidate action potential was determined to be an action potential if the value of R was greater than 0.7. The candidate action potentials that pass this criteria are then stored in a different set along with their timestamps for purposes of comparison.

2.6 Metrics used for Quantification of the Detection Process

Metrics used to quantify the detection process in simulated signals (both manual and automated) are explained below:

$$Sensitivity\ \%\ (S) = \frac{TP}{N} \times 100$$

where TP denotes the number of true positives and N denotes the total number of action potentials present in the signal (based on prior knowledge).

$$Error\ \%\ (E) = \frac{FP}{TD} \times 100$$

where FP denotes the number of false positives and TD denotes the total number of action potentials detected (TP + FP).

$$Missed\ \%\ (M) = \frac{(N - TP)}{N} \times 100$$

A good detection system must have high sensitivity and low percentage of error and missed action potentials.

CHAPTER 3

RESULTS AND ANALYSIS

3.1 Noise Reduction

3.1.1 Simulated ENG Signals

3.1.1.1 FIR Filtered Signals

The standard deviation of the signal was used as an estimator for noise. The values of standard deviation for FIR filtered simulated ENG signals are given in table 3.1 for all the five signals.

Table 3.1: Standard deviation values for FIR filtered simulated ENG signals

Simulated ENG Signal	SNR (dB)	Standard Deviation (μV)
Signal 1	10	4.89
Signal 2	7.5	6.32
Signal 3	5	8.42
Signal 4	2.5	10.82
Signal 5	0	14.53

3.1.1.2 DWT Denoised Signals

Table 3.2 shows standard deviation values for DWT denoised signals as percentages of standard deviation before denoising for all 5 wavelets used under two different levels of decomposition used. Comparison between different wavelets at level 4 and 5 are shown in the figures 3.1 and 3.2 respectively whereas figure 3.3 shows the comparison between levels 4 and 5, where values were averaged across all 5 wavelets.

Table 3.2: Standard deviation values of all the DWT denoised simulated ENG signals given as percentage of standard deviation before denoising

Parameters used in denoising	Standard Deviation (%)				
	Signal 1 (10 dB)	Signal 2 (7.5 dB)	Signal 3 (5 dB)	Signal 4 (2.5 dB)	Signal 5 (0 dB)
level 4 'db4'	41.10	34.34	29.93	27.17	25.74
level 4 'sym7'	41.31	34.65	30.17	27.45	25.95
level 4 'haar'	40.49	33.86	29.57	27.17	25.74
level 4 'bior 3.5'	45.19	39.24	35.15	32.62	31.11
level 4 'bior 3.7'	44.58	38.29	34.32	31.52	29.73
level 5 'db4'	37.22	29.27	23.75	20.33	18.51
level 5 'sym7'	37.42	29.59	24.23	20.70	18.72
level 5 'haar'	36.40	28.80	23.40	20.33	18.44
level 5 'bior 3.5'	42.54	36.08	31.24	28.19	26.08
level 5 'bior 3.7'	42.13	34.97	30.29	26.89	24.50

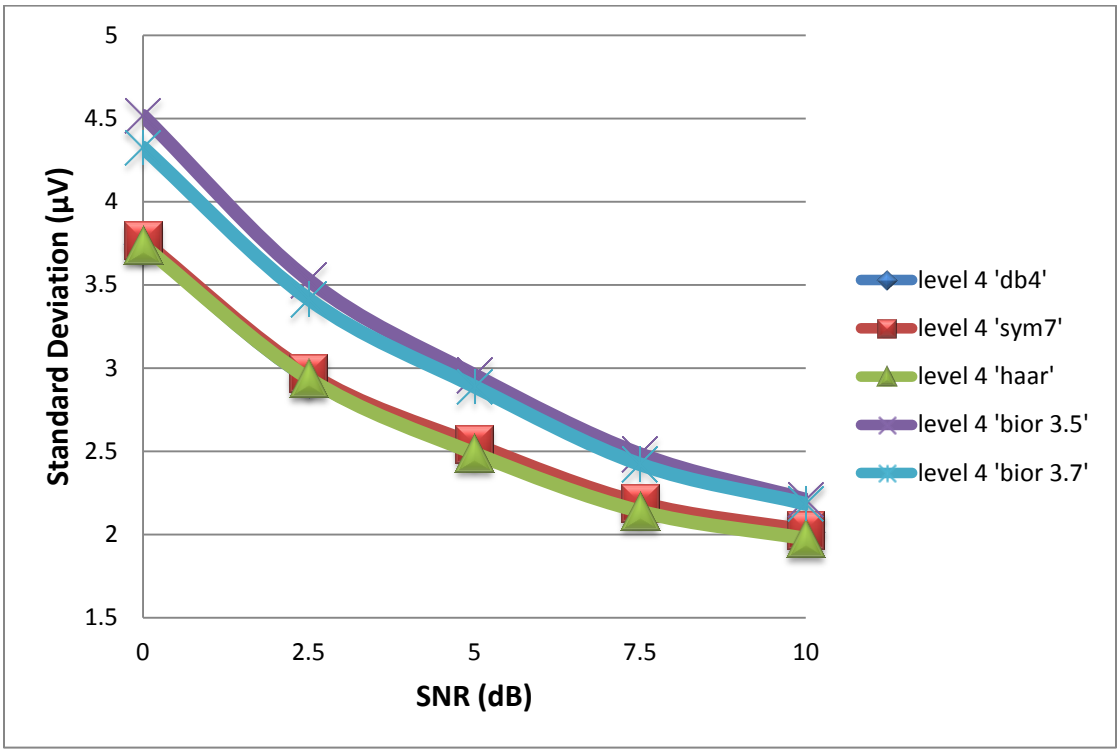

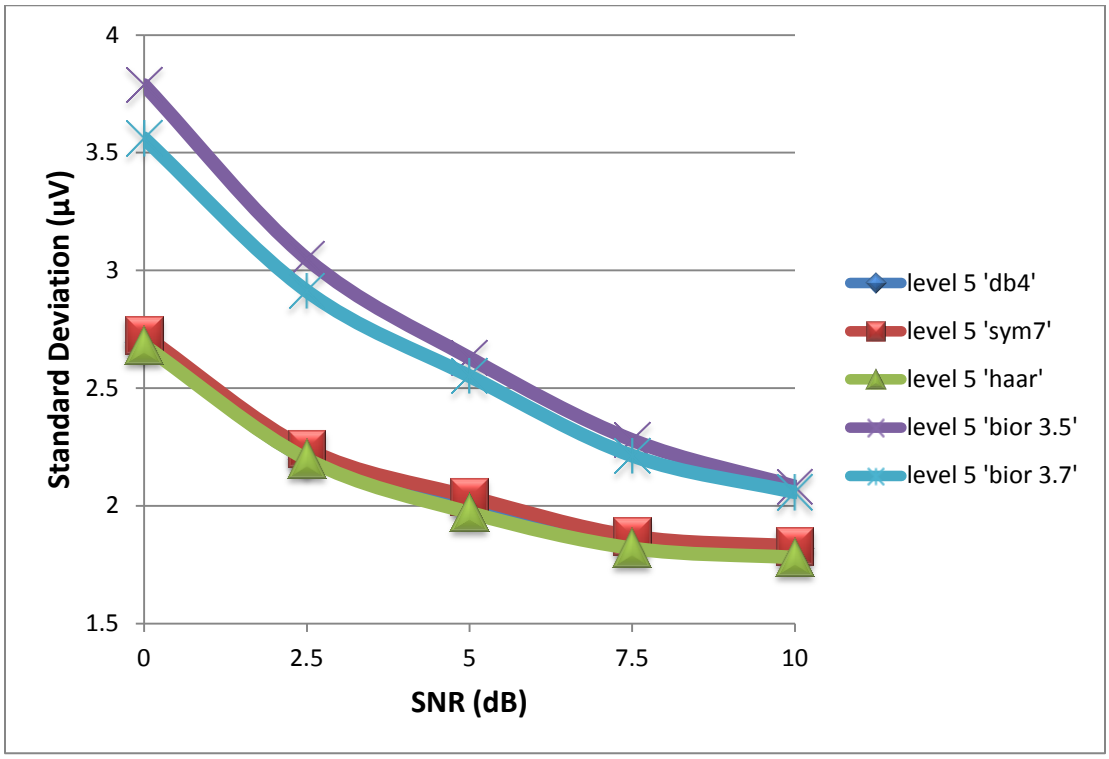

Figure 3.1: Comparison of different wavelets at level 4 and level 5 DWT decomposition

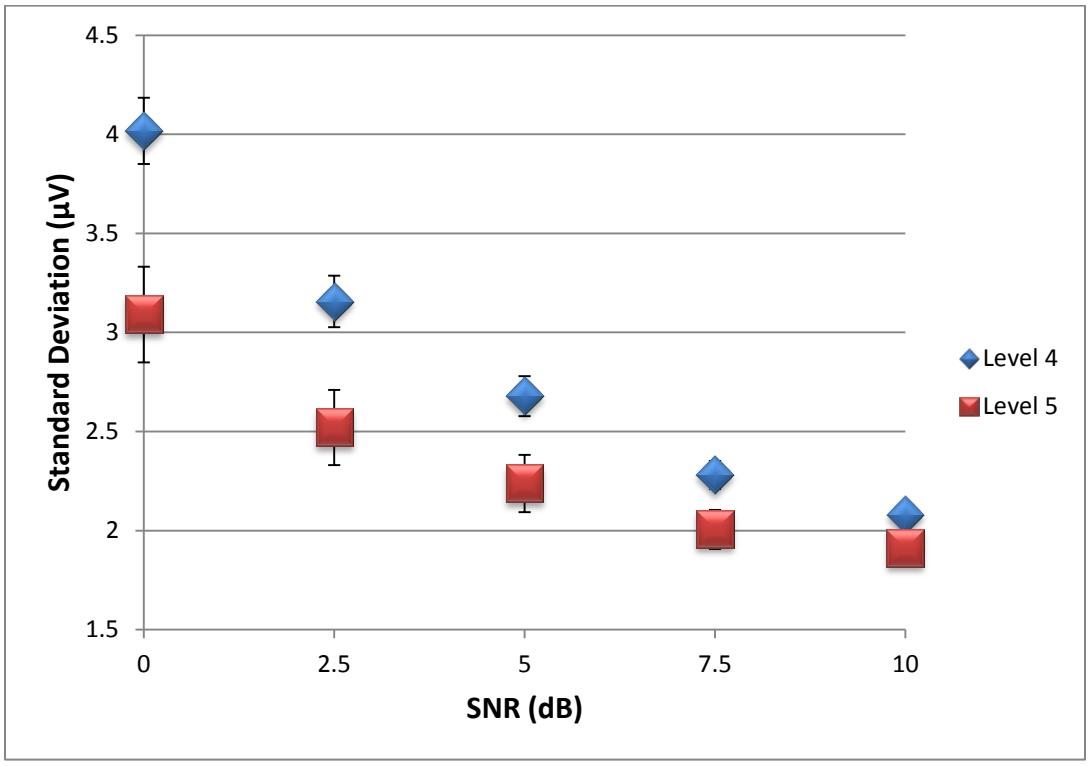

Figure 3.2: Comparison of noise reduction between level 4 and level 5 DWT denoising. Values are averaged across all wavelets used. Error bars represent the standard deviation of values from mean

From figure 3.1 it can be seen that at both levels 4 and 5, wavelets 'db4', 'sym7' and 'haar' reduce noise better than the other two wavelets 'bior 3.5' and 'bior 3.7'.In figure 3.3, mean value of standard deviation across all the wavelets are compared between level 4 and level 5 DWT denoising. Noise in level 5 denoised signals was significantly lesser than that of level 4 denoised signals (*p-value = 0.023*).

3.1.1.3 Statistical Comparison

Statistical comparisons were made between FIR filtering, level 4 DWT denoising and level 5 DWT denoising. One way ANOVA was performed and the results are presented in table 3.3. p-value was calculated to be 0.00089 which is less than 0.05 therefore, considered to be statistically significant. Tukey's HSD test was performed and means of FIR vs. level 4 and FIR vs. level 5 were found to be significantly different from each other.

Table 3.3: Statistical comparison between FIR filtering, level 4 DWT and level 5 DWT on simulated ENG signals

Source	SS	df	MS	F	p -value
Variables	137.0213	2	68.5107	13.3212	0.00089681
Error	61.7157	12	5.143		
Total	198.737	14			

3.1.2 Real ENG Recordings

Noise levels are compared between FIR filtered, DWT denoised and Stationary Wavelet Transform (SWT) denoised ENG recordings. 5 recordings (from 16 channels) of approximately 4 minute length (i.e, total of10,000,000 data points) were chosen for analysis. The standard deviation of each channel was calculated and is considered to be an estimate of noise. Mean of values across all 16 channels was calculated for different methods of denoising and is presented in table 3.4 and a graphical representation is given in figure 3.3. For both DWT and SWT denoising methods, 5 level decomposition using symlet 7 wavelet was used for the results shown in table 3.4. This particular combination was chosen because among all possible combinations, this combination produced optimal sensitivity, as shown in section 3.2.

Table 3.4: Mean values of standard deviation for all 5 recordings

	Recording 1 (μV)	Recording 2 (μV)	Recording 3 (μV)	Recording 4 (μV)	Recording 5 (μV)
FIR	10.13 ± 2.06	9.46 ± 3.33	7.58 ± 1.20	7.82 ± 1.00	7.67 ± 1.47
DWT	4.00 ± 1.74	4.81 ± 2.16	2.59 ± 0.72	3.30 ± 0.99	3.05 ± 0.75
SWT	3.92 ± 1.73	4.72 ± 2.13	2.53 ± 0.71	3.21 ± 0.98	2.97 ± 0.74

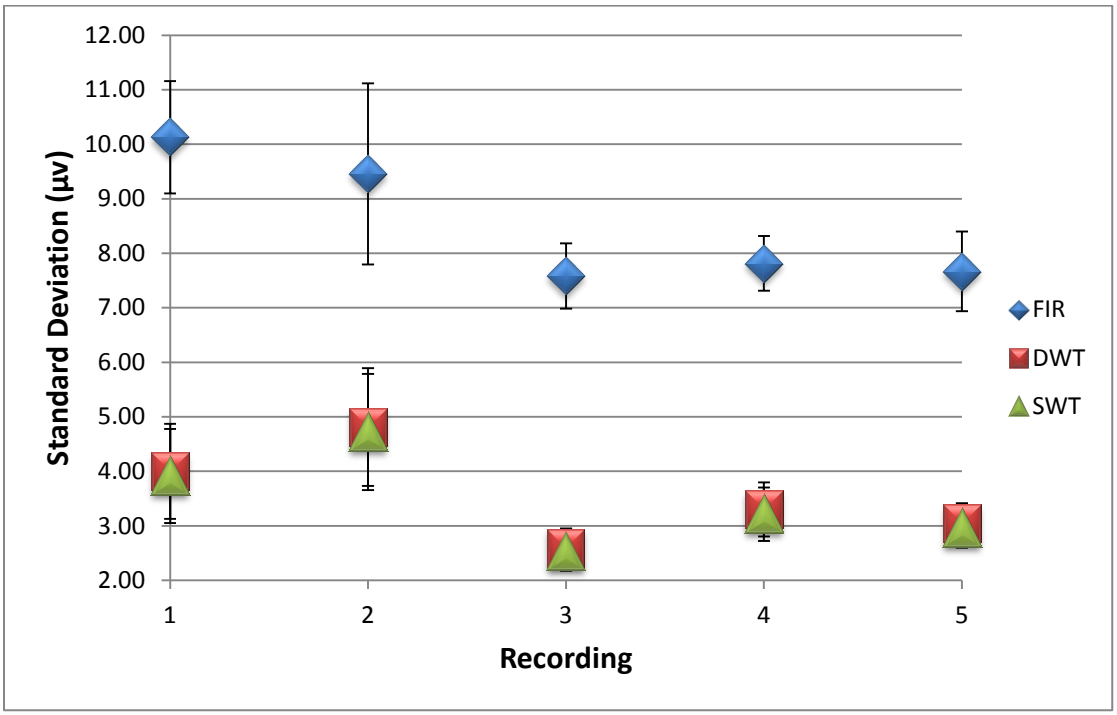

Figure 3.3: Comparison of standard deviation values for ENG recordings under different denoising methods (FIR: Filtered using Finite Impulse Response Filters; DWT: Denoised using Discrete Wavelet Transform; SWT: Denoised using Stationary Wavelet Transform)

A statistical comparison of the three methods of denoising was done similar to the one done for simulated ENG signals and the results of which are presented in table 3.5. one way ANOVA was performed and the p-value was calculated to be 3.11 E -06, which is considered significant. A tukey's HSD post-hoc test was performed and the means of FIR vs. DWT and the means of FIR vs. SWT were found to be significantly different.

Table 3.5: Statistical comparison between FIR filtering, DWT and SWT denoising on real ENG recordings

Source	SS	df	MS	F	p -value
Variables	84.08	2	42.04	43.64	3.11 E -06
Error	11.56	12	0.9635		
Total	95.65	14			

3.1.3 Visual comparison

3.1.3.1 Simulated ENG Signals

Plots of two simulated signals (signal 2 and signal 4) denoised using different methods are shown from figure 3.4 to figure 3.9.

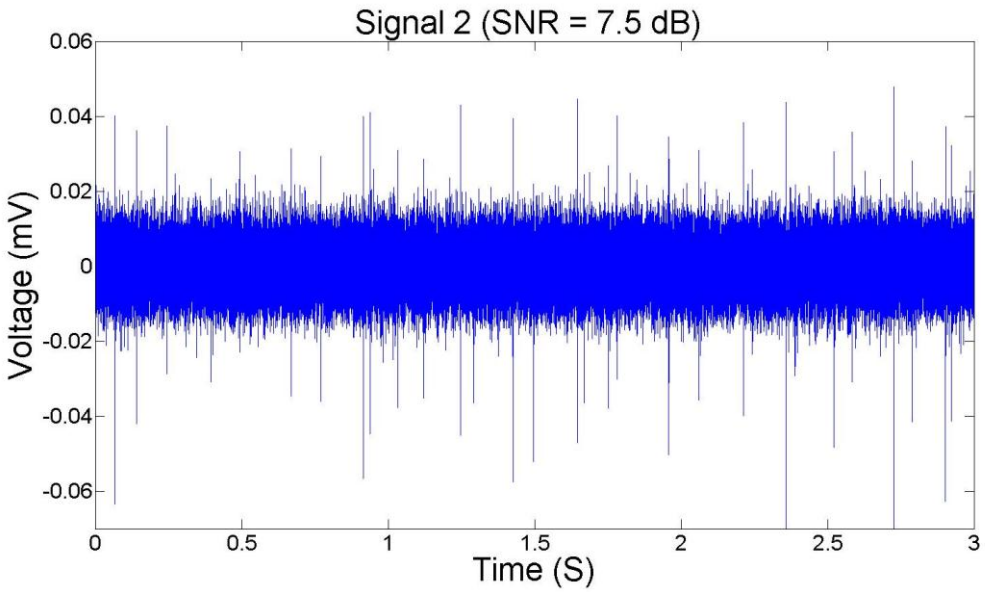

Figure 3.4: A segment of simulated signal 2 filtered using an FIR filter

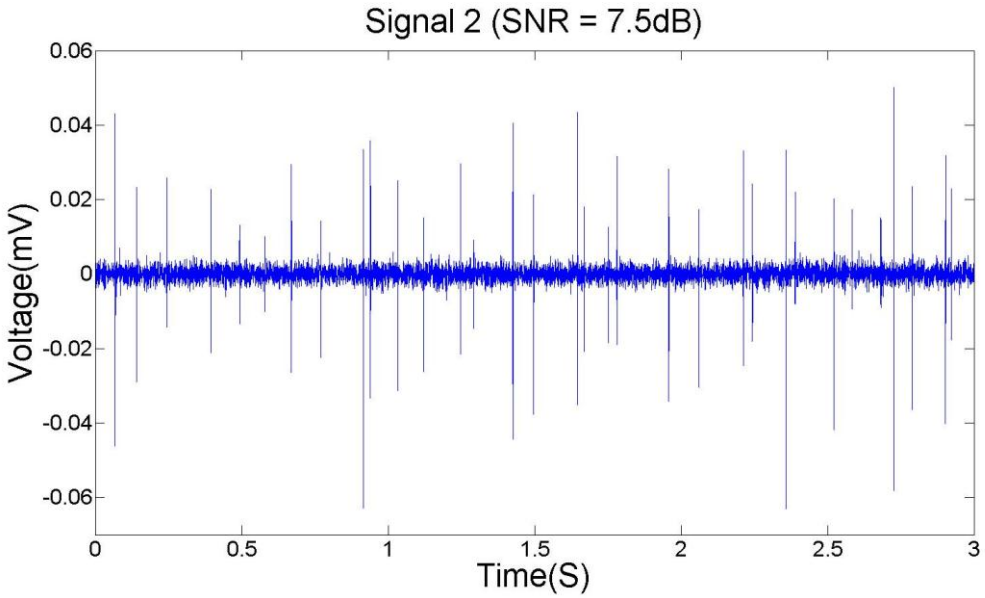

Figure 3.5: Same segment of signal 2 as in figure 3.4 denoised using level 4, 'db4' DWT

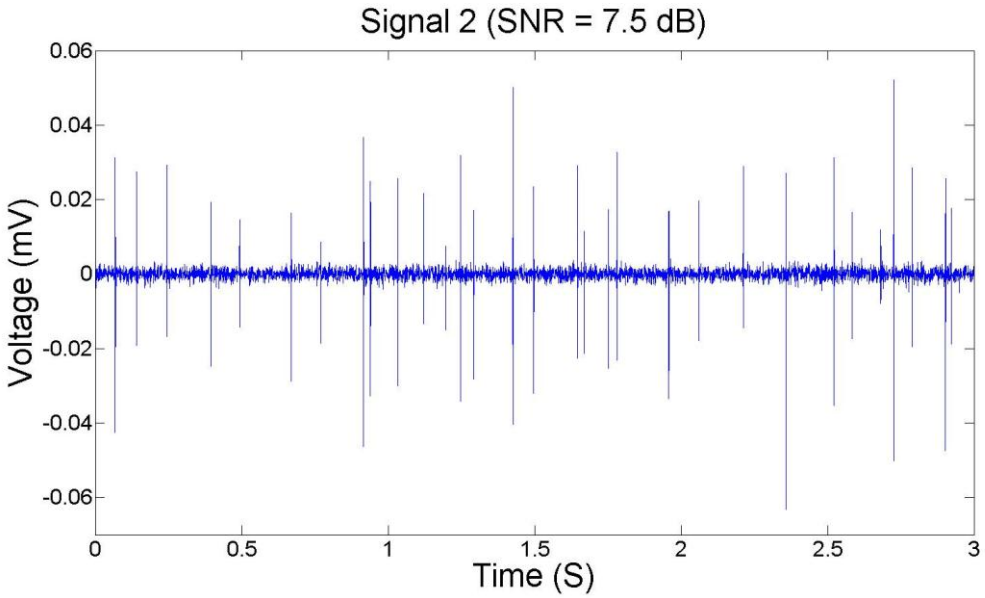

Figure 3.6: Same signal of signal 2 as in figure 3.4 denoised using level 5, 'sym7' DWT

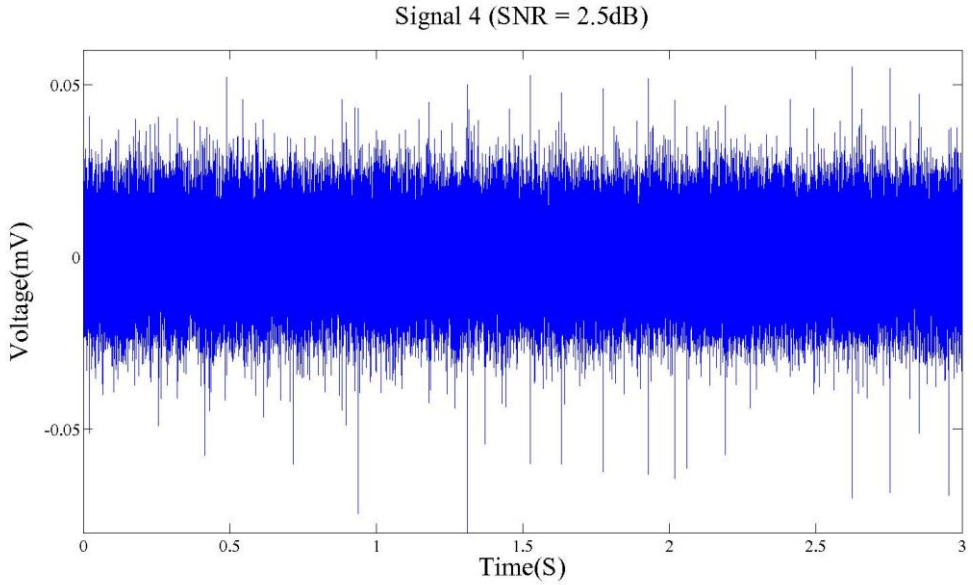

Figure 3.7: A segment of simulated signal 4 filtered using an FIR filter

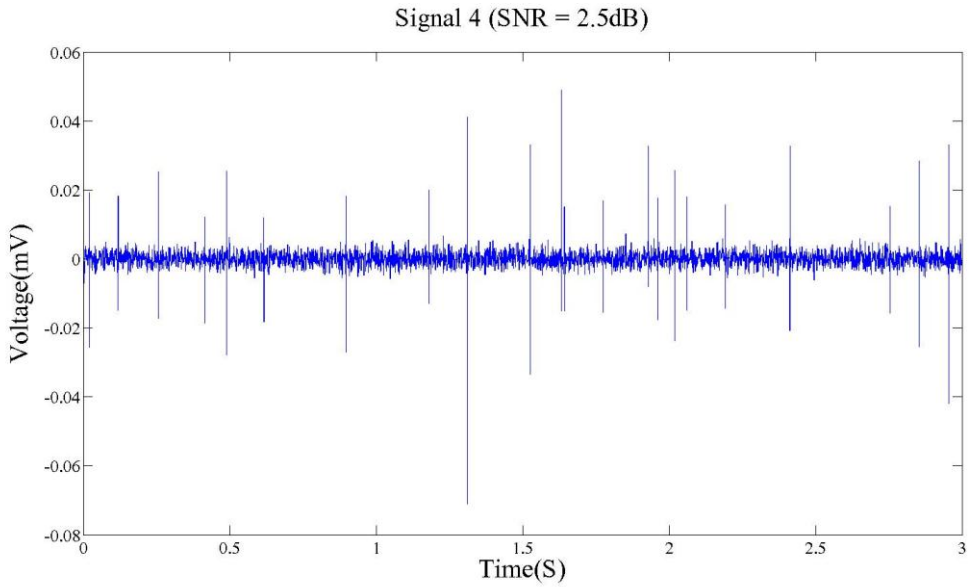

Figure 3.8: Same signal of signal 4 as in figure 3.7 denoised using level 4, ‘haar’ DWT

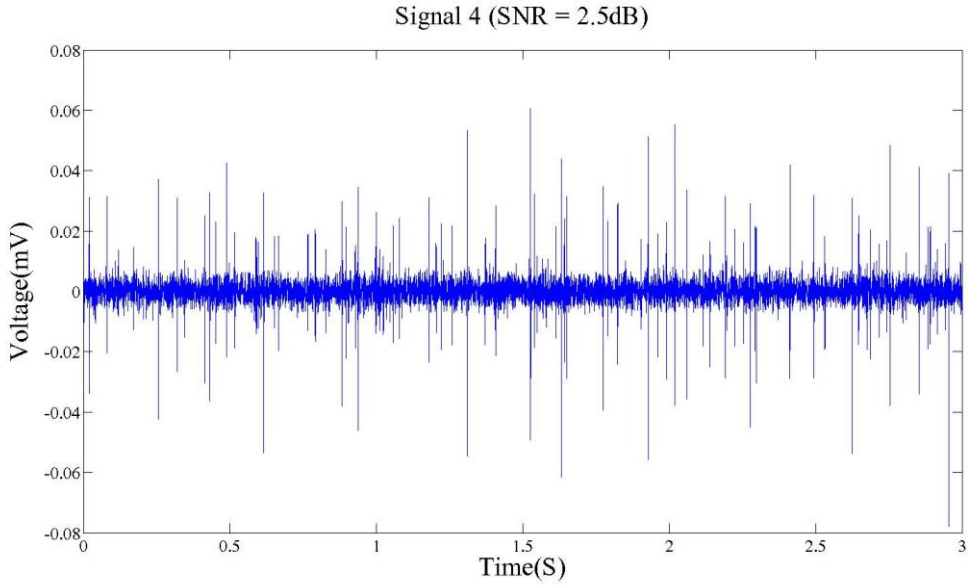

Figure 3.9: Same signal of signal 4 as in figure 3.7 denoised using level 5, ‘bior 3.7’ DWT

3.1.3.2 Real ENG Recordings

Plots of a segment of an ENG recording (Recording 1, Channel 16) denoised using different methods are shown from figure 3.10 to 3.12.

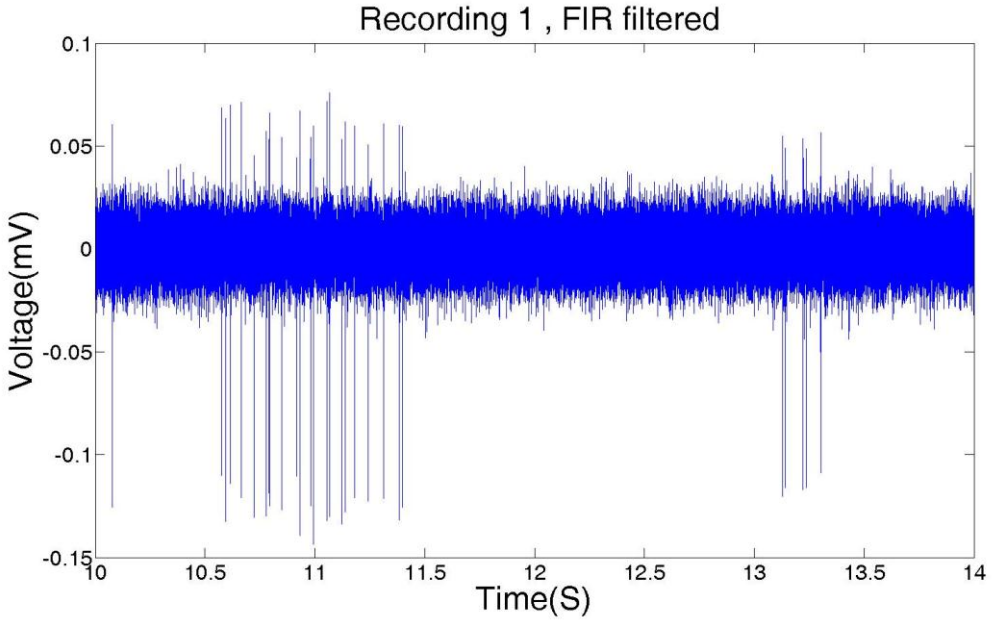

Figure 3.10: A segment of ENG recording filtered using an FIR filter

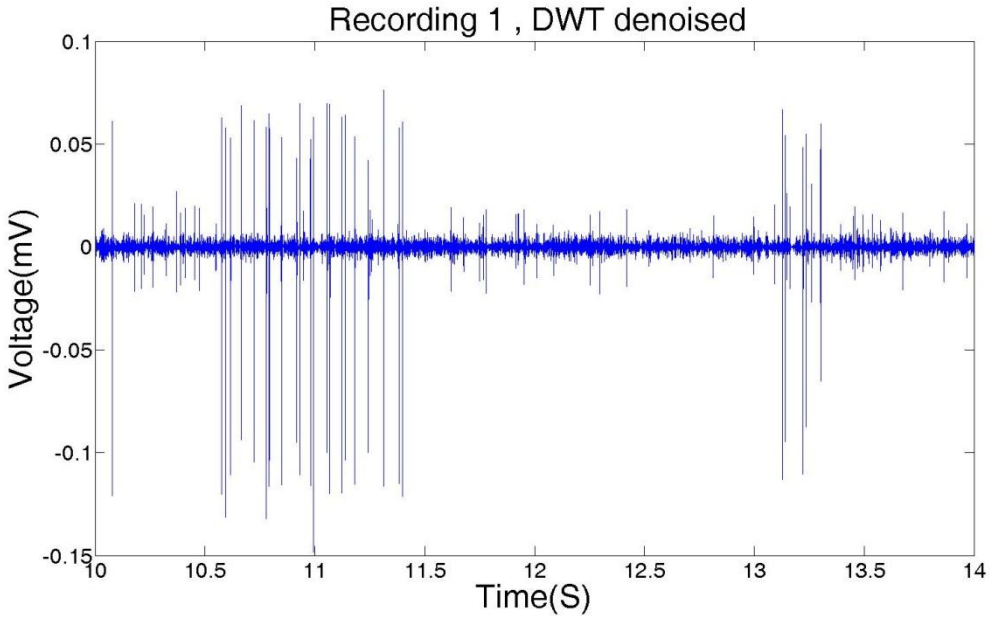

Figure 3.11: Same segment as in figure 3.10 denoised using DWT (level 5, 'sym7')

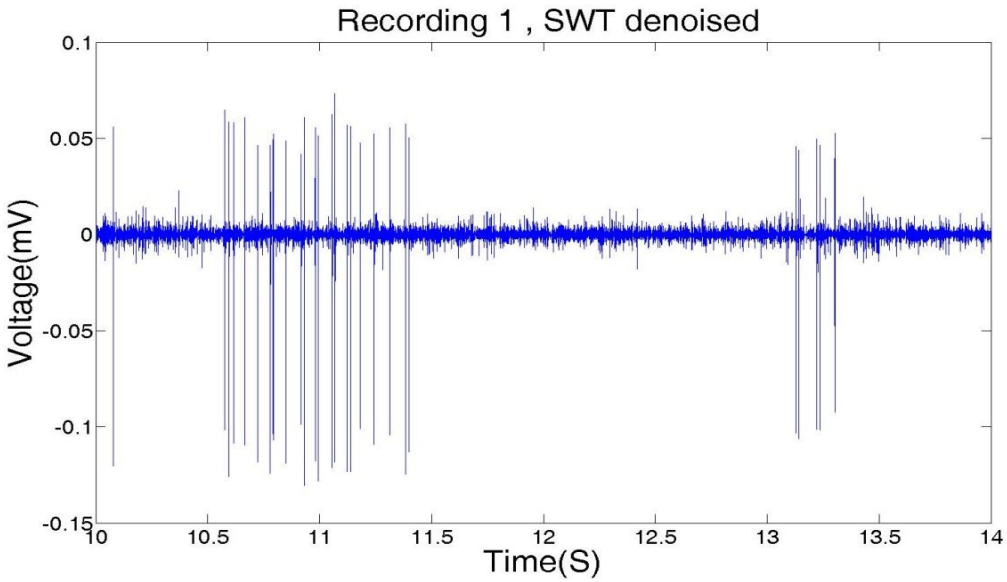

Figure 3.12: Same segment as in figure 3.10 denoised using SWT (level 5, 'sym7')

3.2 Detection of Action Potentials in Simulated ENG Signal

3.2.1 Manual Detection

3.2.1.1 FIR Filtered Signals

The performance of a trained scorer (estimated training period of 2 years) on 5 simulated signals was analyzed and was quantized using the four parameters mentioned in the previous chapter (Section 2.6) namely, Sensitivity (S), Error (E), Missed (M).The results for the 5 signals are provided in table 3.6.

Table 3.6: Results of Manual Detection on FIR filtered Simulated ENG Signals

Signal (SNR)	Sensitivity (S)%	Error (E)%	Missed (M)%
Signal 1 (10 dB)	79.87	0.47	20.13
Signal 2 (7.5 dB)	61.09	0.23	38.91
Signal 3 (5 dB)	49.14	0.00	50.86
Signal 4 (2.5 dB)	30.86	0.84	69.14
Signal 5 (0 dB)	12.48	0.96	87.52

3.2.1.2 DWT Denoised Signals

The performance of the same trained scorer on DWT denoised versions of the simulated signals was analyzed. Results were compared between all combinations of the two levels of denoising and 5 wavelets used. The numerical results are provided in table 3.7 while bar graphs of sensitivity and error of detection for 2 of the 5 signals are given in figures 3.13 and 3.14.

Table 3.7 Results of Manual Detection on DWT Denoised Simulated ENG Signals

Parameter Used for Denoising	**Sensitivity (S) %**				
	Signal 1 (10 dB)	**Signal 2 (7.5 dB)**	**Signal 3 (5 dB)**	**Signal 4 (2.5 dB)**	**Signal 5 (0 dB)**
level 4 'db4'	66.16	61.23	41.70	28.26	15.64
level 4 'sym7'	79.75	63.52	40.32	32.16	19.39
level 4 'haar'	76.98	63.81	49.03	32.16	13.45
level 4 'bior 3.5'	79.62	79.40	65.41	52.73	35.76
level 4 'bior 3.7'	90.57	77.97	74.57	63.02	46.42
level 5 'db4'	73.08	50.79	40.89	26.56	16.24
level 5 'sym7'	76.73	63.38	51.89	36.59	18.91
level 5 'haar'	77.61	65.95	51.66	35.94	15.64
level 5 'bior 3.5'	58.62	74.96	40.09	48.83	42.79
level 5 'bior 3.7'	77.11	60.66	71.59	53.26	45.21

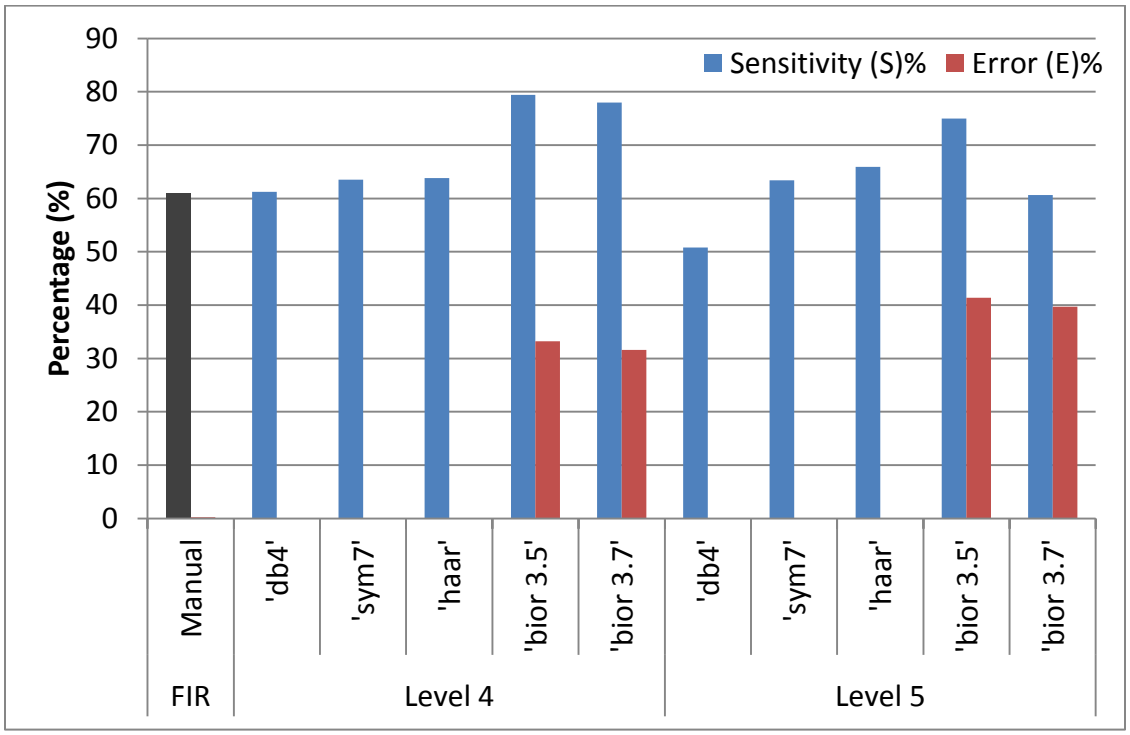

Figure 3.13: Results of Manual Detection in DWT Denoised Simulated ENG Signal 2 (7.5 dB)

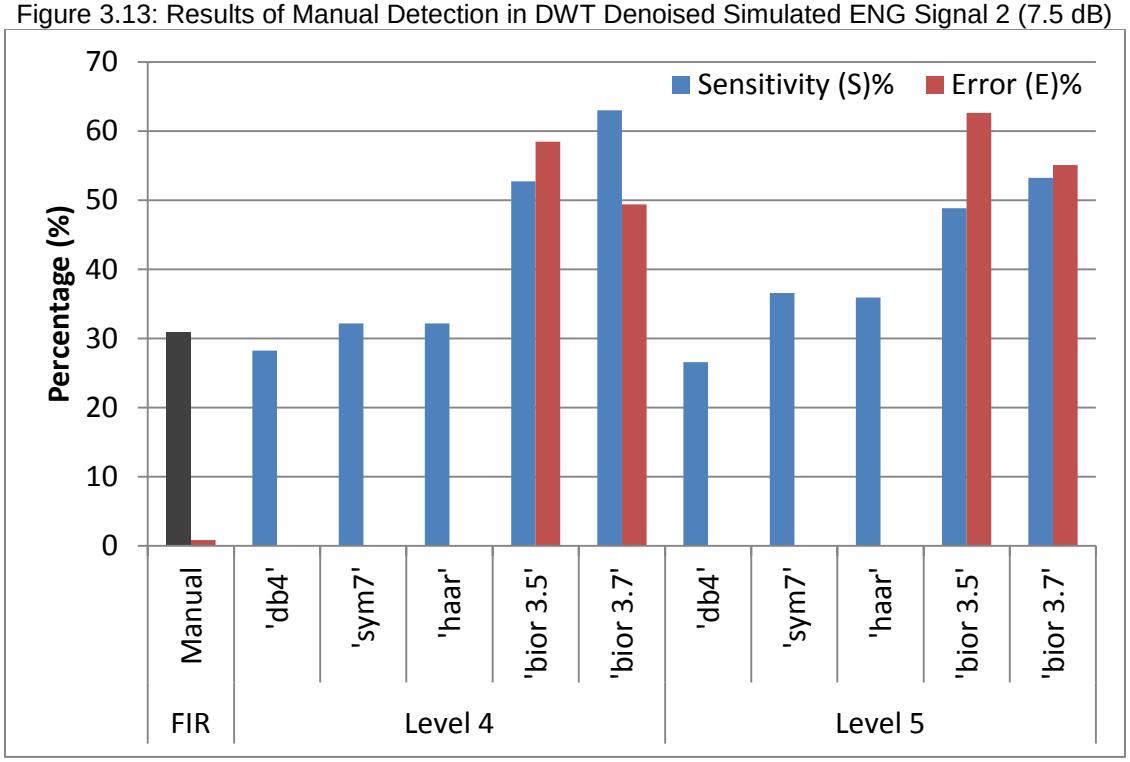

Figure 3.14: Results of Manual Detection in DWT Denoised Simulated ENG signal 4 (2.5 dB)

3.2.2 Automatic Detection

3.2.2.1 FIR Filtered Signals

Performance of the automatic detection algorithm was tested with the FIR filtered simulated signals and the results are presented similar to manual detection. The results of 3 parameters Sensitivity (S), Error (E) and percentage Missed (M) for all the 5 simulated signals are presented in table 3.8 and a graph showing sensitivity of automatic detection is shown in figure 3.15.

Table 3.8 Results of automatic detection on FIR Filtered Simulated ENG Signals

	Sensitivity (S)%	**Error (E)%**	**Missed (M)%**
Signal 1	89.94	1.92	10.06
Signal 2	82.69	2.53	17.31
Signal 3	72.97	3.04	27.03
Signal 4	61.07	6.57	38.93
Signal 5	46.91	7.86	53.09

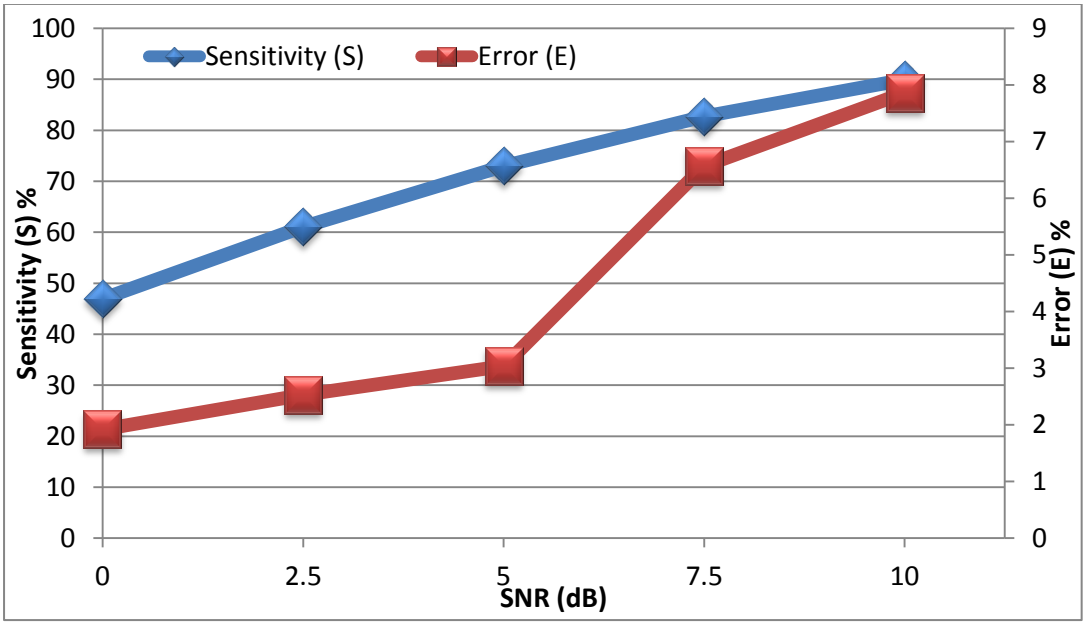

Figure 3.15: Graph showing sensitivity and error of automatic detection on simulated ENG signals when FIR filtering is used to denoise the signal

3.2.2.2 DWT Denoised Signals

Performance of automatic detection was analyzed on the simulated ENG signals that were denoised using DWT. All combinations of two denoising levels and five wavelets were utilized in all 5 files and their results were compared. Sensitivity of the automatic detection on all 5 files and in all combinations is tabulated and presented in table 3.9.

Table 3.9: Results of Automatic Detection on DWT Denoised simulated ENG signals

Parameters Used for Denoising	**Sensitivity (S) %**				
	Signal 1 (10 dB)	**Signal 2 (7.5 dB)**	**Signal 3 (5 dB)**	**Signal 4 (2.5 dB)**	**Signal 5 (0 dB)**
level 4 'db4'	76.98	62.23	49.37	32.81	15.03
level 4 'sym7'	78.74	64.38	53.15	36.59	18.30
level 4 'haar'	75.35	62.66	47.19	32.81	13.45
level 4 'bior 3.5'	87.17	77.54	64.15	54.04	37.21
level 4 'bior 3.7'	88.81	76.68	66.09	54.30	38.42
level 5 'db4'	78.74	63.66	50.40	33.72	15.27
level 5 'sym7'	80.50	65.81	54.18	36.59	19.15
level 5 'haar'	75.85	63.23	48.22	32.16	13.21
level 5 'bior 3.5'	83.52	71.53	57.04	42.97	28.12
level 5 'bior 3.7'	85.41	72.10	61.05	49.61	32.61

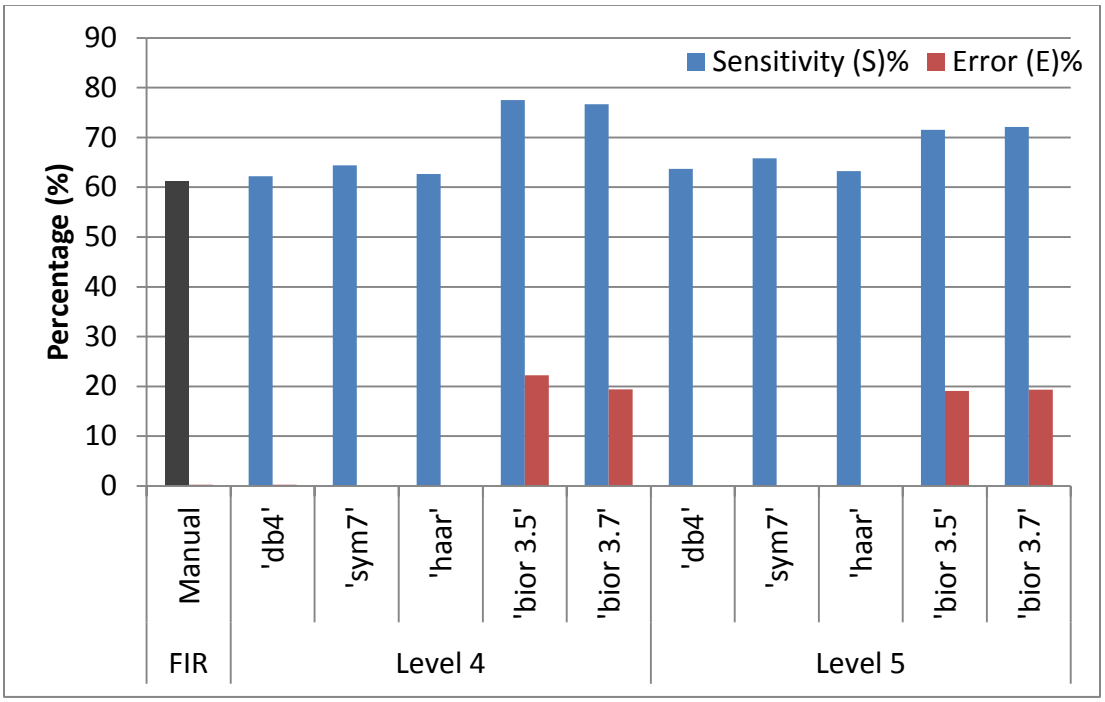

Figure 3.16: Results of Automatic Detection in DWT denoised simulated ENG signal 2 (7.5 dB)

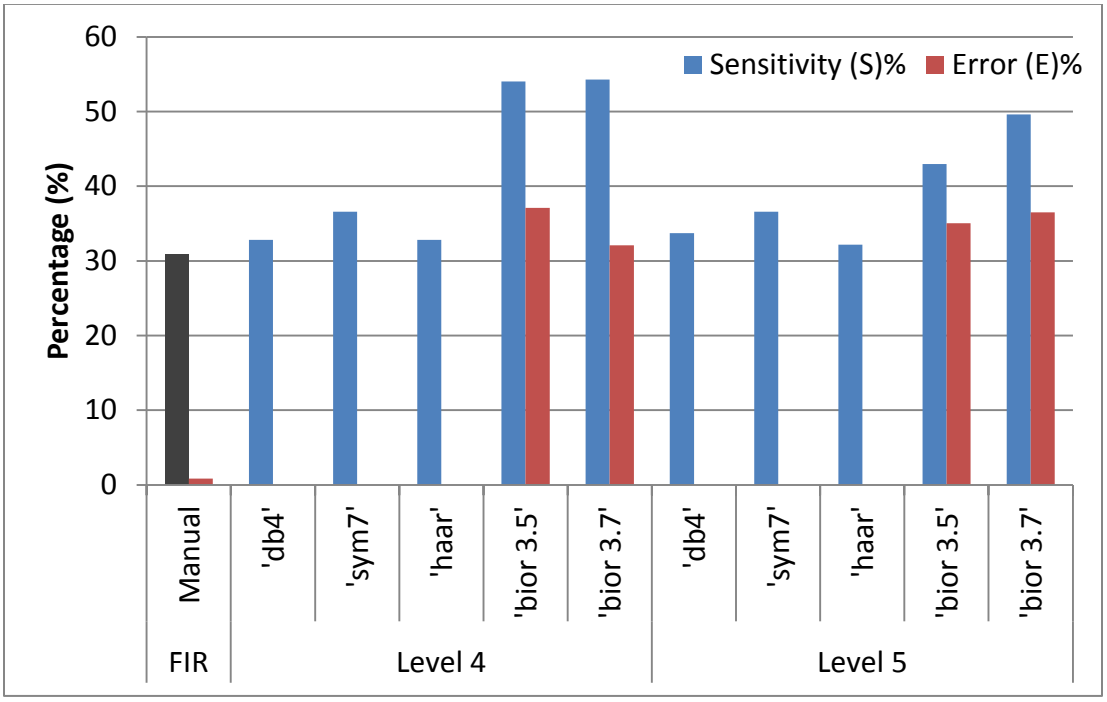

Figure 3.17: Results of Automatic detection in DWT denoised simulated ENG signal 4 (2.5 dB)

3.2.2.3 SWT Denoised Signals

Performance of the automatic template matching algorithm was analyzed on SWT denoised files in a similar way to DWT files. Percentage sensitivity of the algorithm was calculated on simulated signals denoised using all possible combinations of the two levels of denoising and five wavelets and the results are tabulated in table 3.10.

Table 3.10: Performance of Automatic detection in SWT Denoised Simulated ENG Signals

Parameters Used for Denoising	**Sensitivity (S) %**				
	Signal 1 (10 dB)	**Signal 2 (7.5 dB)**	**Signal 3 (5 dB)**	**Signal 4 (2.5 dB)**	**Signal 5 (0 dB)**
level 4 'db4'	93.96	80.69	68.27	57.68	41.21
level 4 'sym7'	95.47	84.69	72.05	61.46	46.30
level 4 'haar'	94.72	84.12	70.10	60.68	45.09
level 4 'bior 3.5'	96.35	90.27	79.95	67.84	53.33
level 4 'bior 3.7'	96.23	89.70	79.95	67.97	53.94
level 5 'db4'	95.72	83.69	70.90	60.94	45.94
level 5 'sym7'	97.23	85.98	72.85	62.76	50.91
level 5 'haar'	95.72	83.83	69.76	60.68	46.06
level 5 'bior 3.5'	96.73	90.99	81.44	69.66	56.48
level 5 'bior 3.7'	96.60	90.70	80.53	69.01	56.85

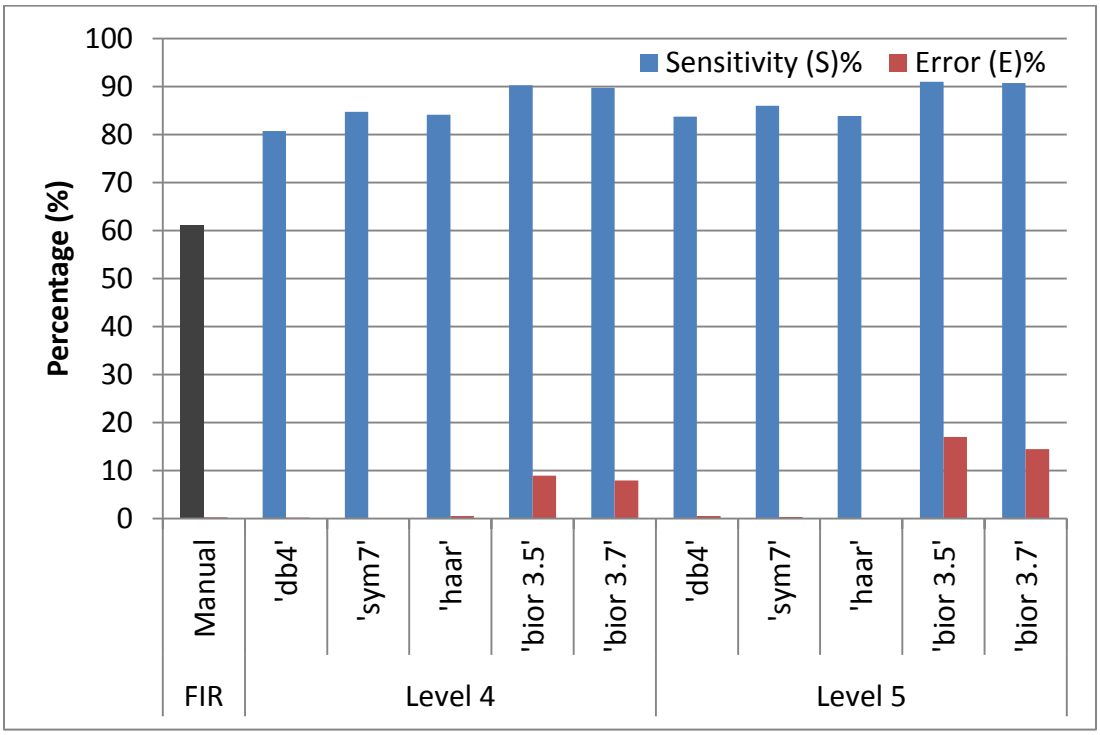

Figure 3.18: Performance of Automatic detection in SWT denoised simulated signal 2 (7.5 dB)

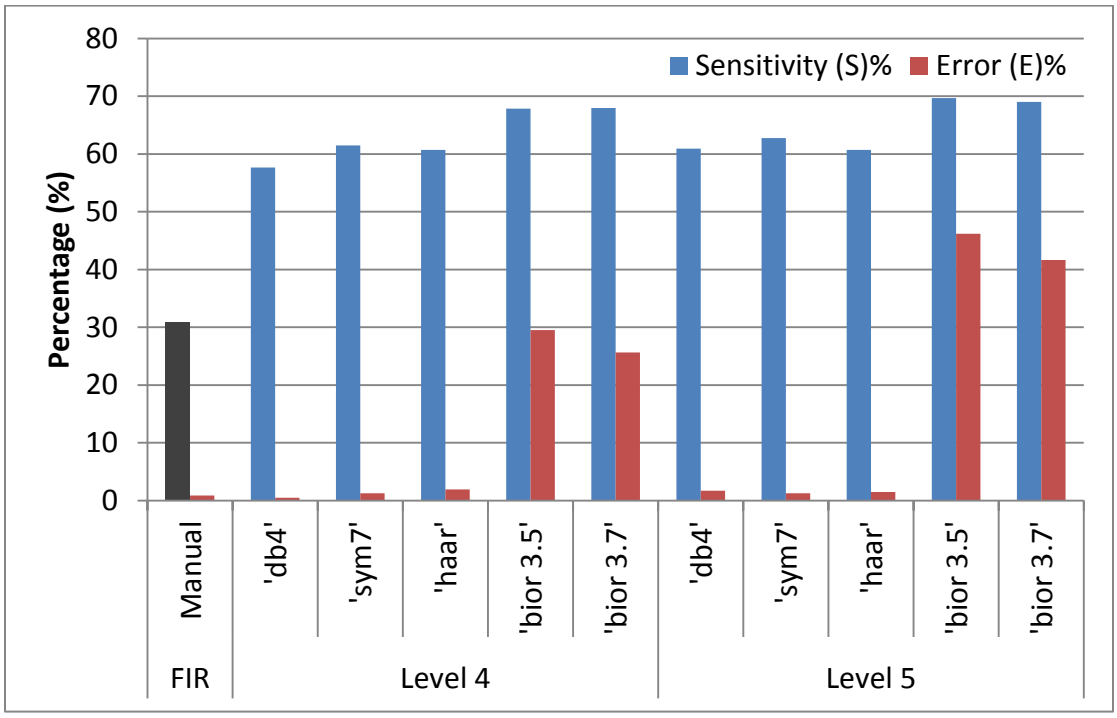

Figure 3.19: Performance of automatic detection in SWT denoised simulated signal 4 (2.5 dB)

3.2.3 Comparison of Detection Modes

Five different modes of detection were compared. Namely, manual detection on FIR filtered signals, manual detection on DWT denoised signals, automatic detection on FIR filtered signals, automatic detection on DWT denoised signals and automatic detection on SWT denoised signals. For DWT and SWT denoised signals, level 5 denoising with 'sym7' wavelet was chosen for comparison purposes as this combination consistently provided the best results when compared with all the other combinations. The value of sensitivity for all the five simulated signals detected using the above mentioned 5 modes are given in the form of a table in table 3.11 and is also shown as a graph in figure 3.20. The average sensitivity and error of the detection modes (averaged across all SNRs) are shown in the form of a graph in figure 3.21.

Table 3.11: Comparison of the sensitivity of five detection modes

Simulated Signal	**Sensitivity (S)%**				
	FIR/manual	**FIR/auto**	**DWT/manual**	**DWT/auto**	**SWT/auto**
Signal 1 (10 dB)	79.87	89.94	76.73	80.50	97.23
Signal 2 (7.5 dB)	61.09	82.69	63.38	65.81	85.98
Signal 3 (5 dB)	49.14	72.97	51.89	54.18	72.85
Signal 4 (2.5 dB)	30.86	61.07	36.59	36.59	62.76
Signal 5 (0 dB)	12.48	46.91	18.91	19.15	50.91

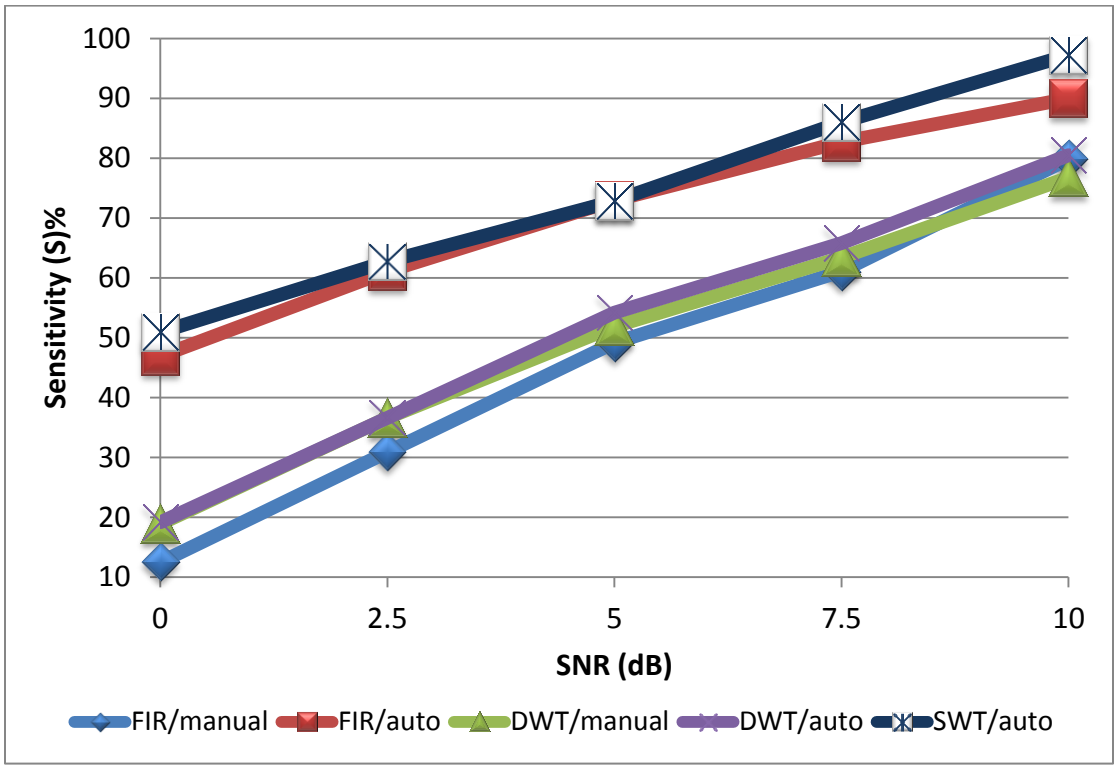

Figure 3.20: Graphical comparison of sensitivity of various detection modes tested using simulated ENG signals

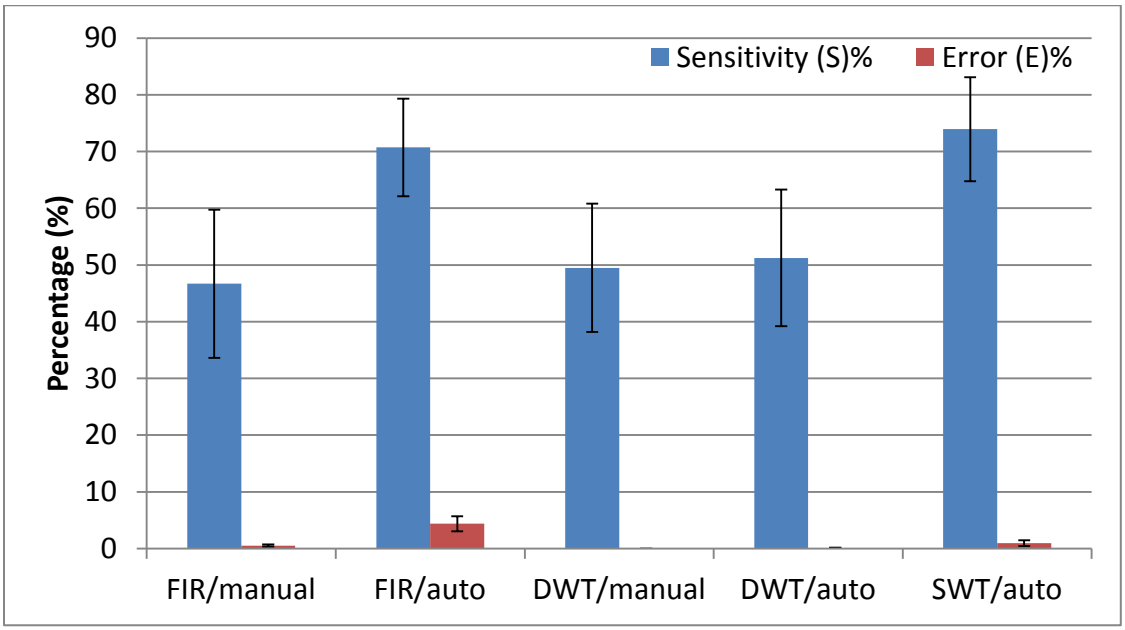

Figure 3.21: Average sensitivity and error of various detection modes. Error bars represent the standard deviation of values from mean

Performance of manual detection was compared with automatic detection for FIR filtered signals as well as DWT denoised signals by performing t-tests and the resulting p-values are given in table 3.12. It can be seen that automatic detection on FIR filtered signals produced significantly better results than manual detection on FIR filtered signals whereas for DWT signals, the difference is not statistically significant.

Table 3.12: Statistical comparison of parameters between manual and automatic detection methods. Statistically significant p-values are marked with an asterisk next to it.

Type of signal	**p-value of t-test**	
	Sensitivity (S)	**Error (E)**
For FIR filtered signals	0.0045*	0.0203*
For DWT denoised signals	0.0705	0.2752

The three denoising methods used, namely FIR filtering, DWT denoising and SWT denoising were compared and the results of the statistical analysis are presented in table 3.13. p-values of t-tests performed are given in the table and the values that are significant are marked with an asterisk.

Table 3.13: Statistical comparison of sensitivity and error of detection between FIR filtering, DWT denoising and SWT denoising. Statistically significant p-values are marked with an asterisk.

Comparison made	**Type of detection**	**p-value of t-test**	
		Sensitivity (S)	**Error (E)**
FIR vs. DWT	Manual	0.1723	0.0192*
	Automatic	0.0036*	0.0240*
FIR vs. SWT	Automatic	0.0595	0.0114*
DWT vs. SWT	Automatic	0.0012*	0.1419

Table 3.14: Comparison summary between the detection modes studied including the comparison of average processing time using MATLAB. TM denotes time taken for manual detection. Processing times are time taken per channel.

Detection Mode	Average processing time	Average Sensitivity	Average Error	Average Missed
FIR/Manual	0.5 s + TM	46.69	0.50	53.31
FIR/Auto	5.8 s	70.72	4.38	29.28
DWT/Manual	0.9 s + TM	49.50	0.00	50.50
DWT/Auto	6.2 s	51.25	0.06	48.75
SWT/Auto	8.9 s	73.95	0.95	26.05

A comparison summary between all the five detection modes tested comparing their average sensitivity, error and missed percentages along with the processing time is given in table 3.14. The processing times provided were the time taken per channel with the average length of a signal being 45 seconds. The computer which was used to compute the processing times had an Intel Xeon Quad Core processor with 8 GB RAM and 2 GHz clock frequency running on Windows XP.

3.3 Detection of Action Potentials in Real ENG recordings

3.3.1 Manual Detection

3.3.1.1 FIR Filtered Recordings

The scores of the trained scorer for the four recordings are shown in table 3.15. The values shown are the sum of all 16 channels for a recording. It is to be noted that these scores were used to compare with all other detection modes. Table 3.16 shows the scores for the same recordings by an inexperienced scorer (estimated experience of 2 months). The scores of an inexperienced scorer was compared with the experienced scorer and the results were classified using 3 parameters namely, Sensitivity, Error and Missed, the values for which are given in table 3.17.

Table 3.15: Scores of an experienced scorer on FIR Filtered ENG recordings. The number of action potentials given is the sum of action potentials detected from all 16 channels in a recording.

Recording	**Total Number of Action Potentials Detected**
Recording 1	1648
Recording 2	520
Recording 3	8052
Recording 4	6214

Table 3.16: Scores of an inexperienced scorer on FIR Filtered ENG Recordings. The number of action potentials given is the sum of action potentials detected from all 16 channels in a recording.

Recording	**Total Number of Action Potentials Detected**
Recording 1	1440
Recording 2	91
Recording 3	5034
Recording 4	5784

Table 3.17: Performance of inexperienced scorer when scores were matched against that of the experienced scorer.

Recording	Sensitivity (S) (%)	Error (E) (%)	Missed (M) (%)
Recording 1	65.78	24.72	34.22
Recording 2	16.73	4.40	83.27
Recording 3	51.11	18.26	48.89
Recording 4	68.91	25.97	31.09
Average	50.63	18.34	49.37

3.3.1.2 DWT Denoised Recordings

The performance of manual detection on DWT denoised recordings was analyzed and compared with the gold standard. The results were quantized using three parameters namely, Sensitivity, Error and Missed and are given in table 3.18. The scoring in this case was performed by the experienced scorer.

Table 3.18: Performance of Manual Detection by experienced scorer on DWT denoised ENG recordings.

Recording	Sensitivity (S) (%)	Error (E) (%)	Missed (M) (%)
Recording 1	84.89	23.55	15.11
Recording 2	69.81	28.26	30.19
Recording 3	52.87	13.98	47.13
Recording 4	62.10	20.82	37.90
Average	67.42	21.66	32.58

3.3.2 Automatic Detection

The performance of automatic detection using the template matching algorithm was examined for FIR filtered, DWT and SWT denoised recordings. The value of correlation threshold (C) chosen was different for the type of denoising used and the basis of their selection are explained under the respective sections below.

3.3.2.1 FIR Filtered Recordings

Correlation threshold was varied from 0.35 to 0.65 in steps of 0.05 in order to find the optimal threshold and the resulting scores were examined for all 4 recordings. The scores were matched against the gold standard and the values of sensitivity and error for all 4 recordings under different thresholds are plotted in the form of a graph in figures 3.22 and 3.23.

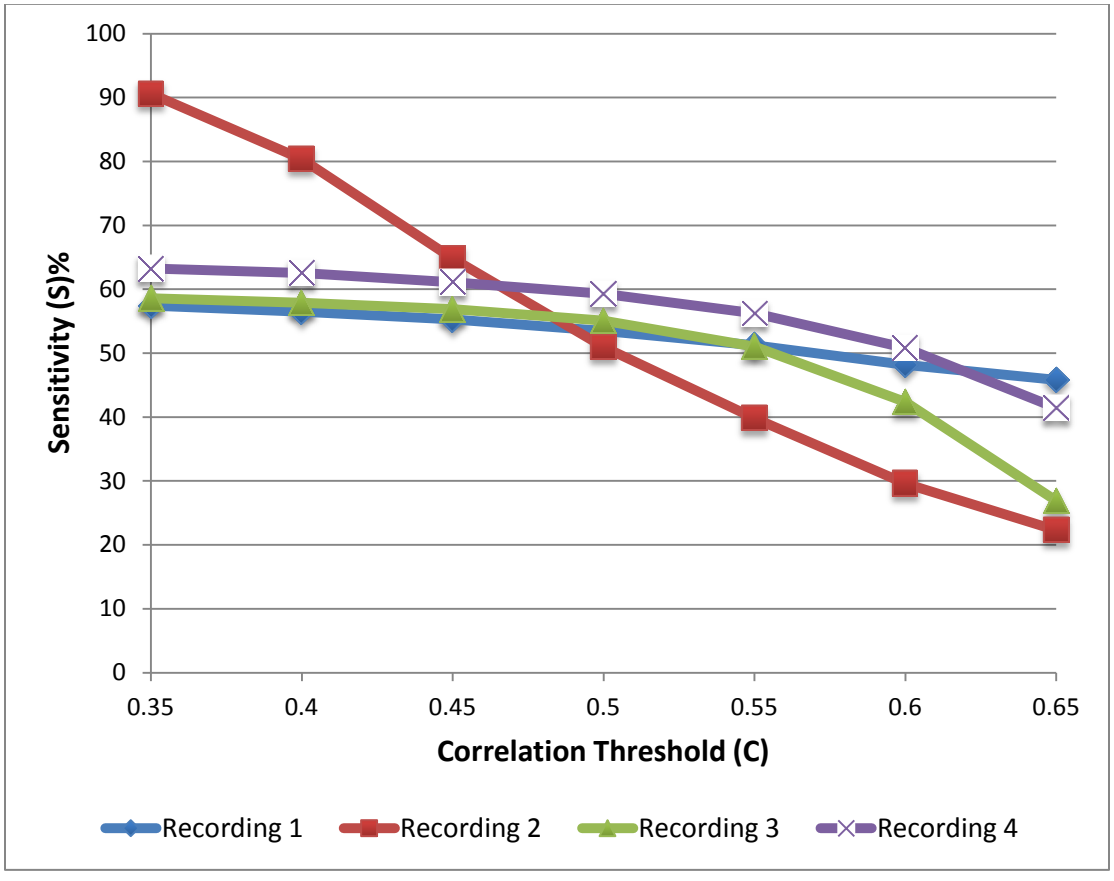

Figure 3.22: Sensitivity of automatic detection under different correlation thresholds on FIR filtered ENG Recordings

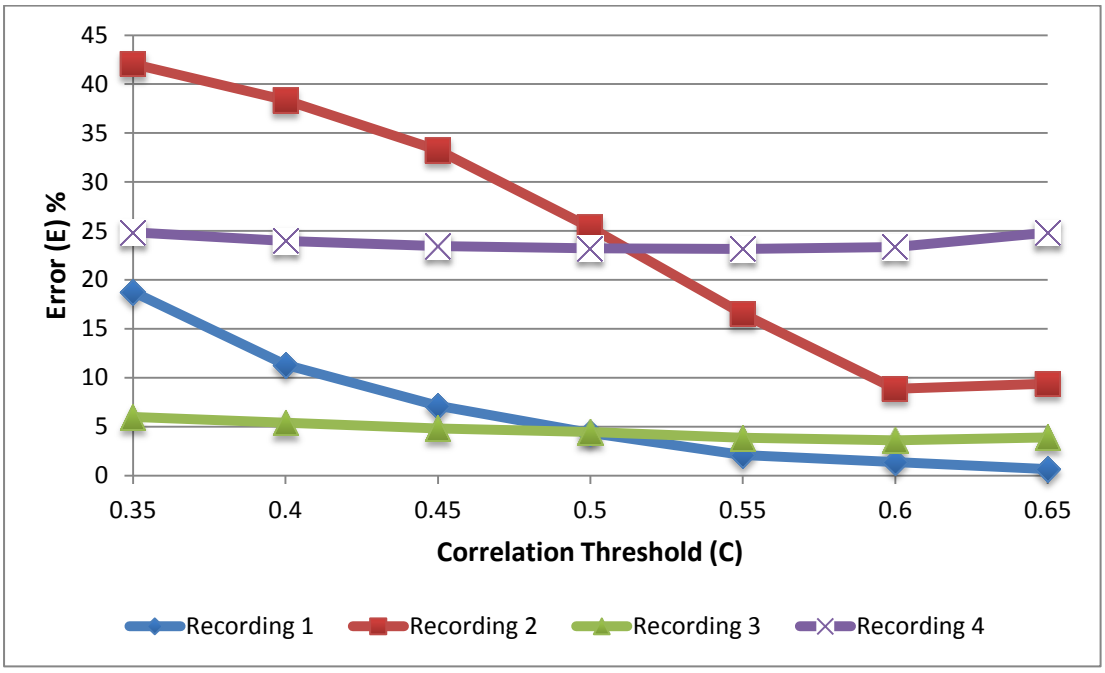

Figure 3.23: Error of automatic detection under different correlation thresholds on FIR filtered ENG Recordings

Based on the average sensitivity and error values (averaged across all 4 recordings), correlation threshold of C = 0.35 was chosen as optimal for FIR filtered signals. The scores of automatic detection performed with the correlation coefficient as 0.35 were compared with the gold standard and the results are given in table 3.19.

Table 3.19: Performance of Automatic Detection on FIR filtered ENG recordings (C = 0.35)

Recording	Sensitivity (S) (%)	Error (E) (%)	Missed (M) (%)
Recording 1	57.46	18.78	42.54
Recording 2	90.58	42.07	9.42
Recording 3	58.58	5.98	41.42
Recording 4	63.23	24.86	36.77
Average	67.46	22.92	32.54

3.3.2.2 DWT Denoised Recordings

Correlation threshold was varied from 0.5 to 0.8 in increments of 0.05 in order to find the optimal threshold and the values of sensitivity and error for each threshold on all recordings are plotted in the form of a graph in figures 3.24 and 3.25. The optimal correlation threshold was chosen as C = 0.5 for DWT denoised recordings. The resulting scores from using such a threshold was compared with the gold standard and are presented in the table 3.20.

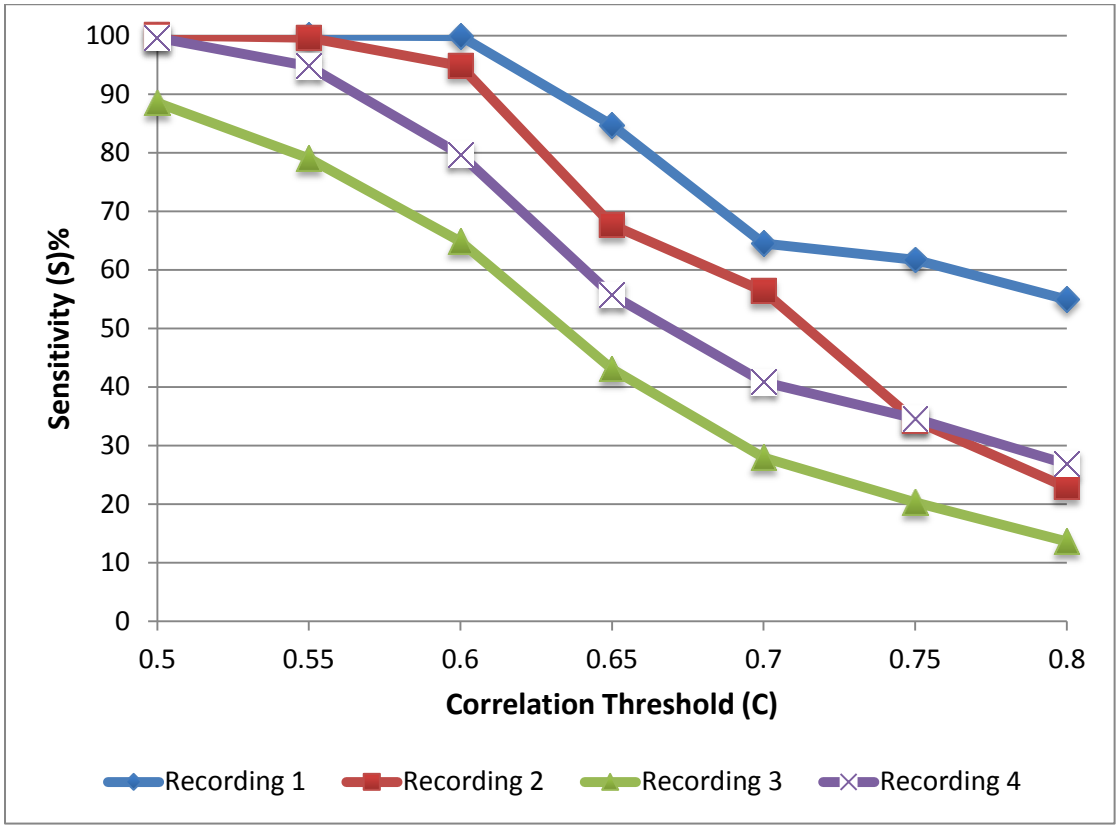

Figure 3.24: Sensitivity of automatic detection under different correlation thresholds on DWT denoised ENG recordings

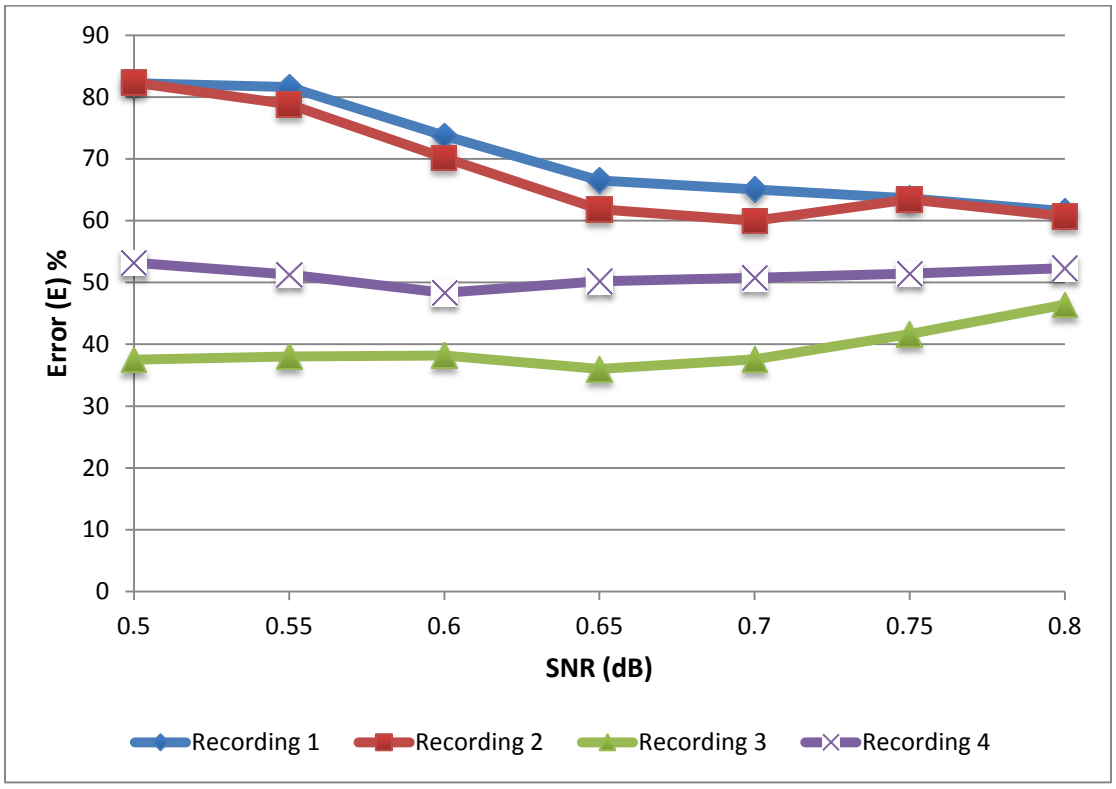

Figure 3.25: Error of automatic detection under different correlation thresholds on DWT denoised ENG recordings

Table 3.20: Performance of Automatic Detection on DWT denoised ENG recordings (C = 0.50)

Recording	Sensitivity (S) (%)	Error (E) (%)	Missed (M) (%)
Recording 1	100.00	82.25	0.00
Recording 2	100.00	82.32	0.00
Recording 3	88.56	37.51	11.44
Recording 4	99.60	53.21	0.40
Average	97.04	63.82	2.96

3.3.2.3 SWT Denoised Recordings

Correlation threshold was varied from 0.50 to 0.80 in increments of 0.05 to find the optimal threshold value. The values of sensitivity and error of detection under different

thresholds for all 4 recordings are presented in the form of a graph in figures 3.26 and 3.27. Based on the average sensitivity, C = 0.50 was chosen as optimal and the results obtained by using this value is presented in table 3.21.

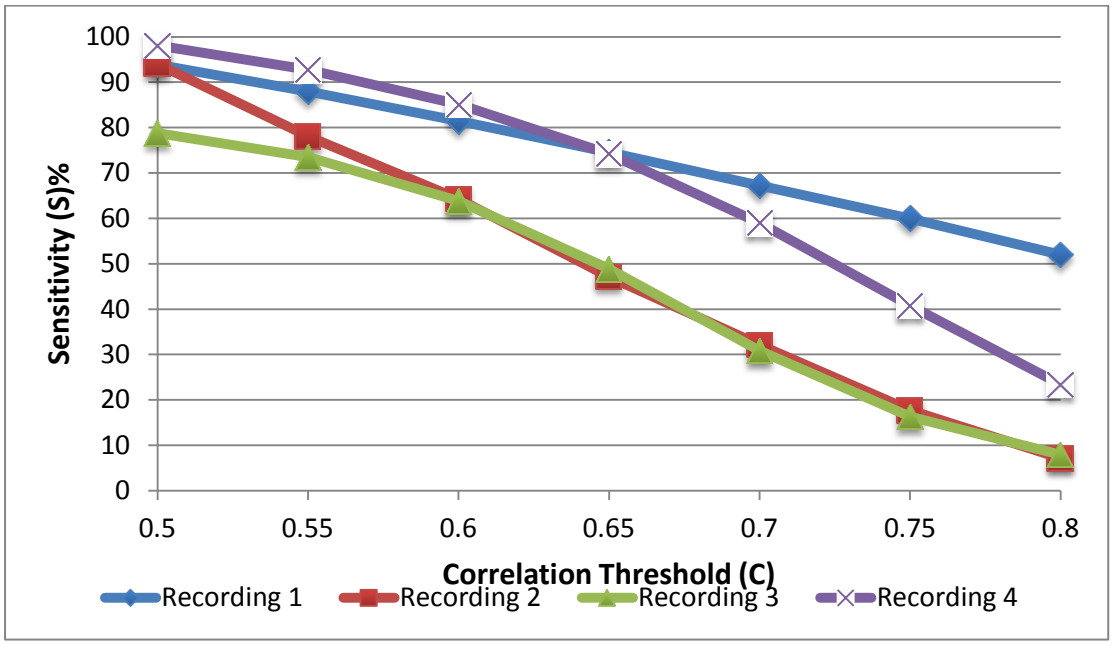

Figure 3.26: Sensitivity of automatic detection under different correlation thresholds on SWT denoised ENG recordings

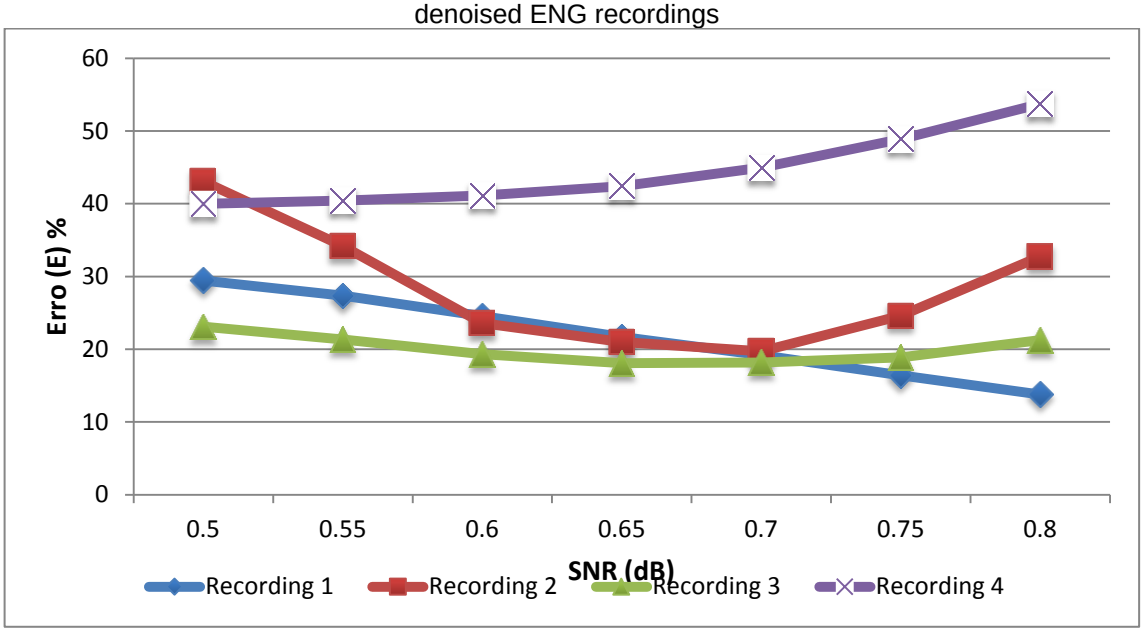

Figure 3.27: Error of automatic detection under different correlation thresholds on SWT denoised ENG recordings

Table 3.21: Performance of Automatic Detection on SWT denoised ENG recordings (C = 0.50)

Recording	Sensitivity (S) (%)	Error (E) (%)	Missed (M) (%)
Recording 1	93.87	29.43	6.13
Recording 2	94.04	43.07	5.96
Recording 3	78.81	23.08	21.19
Recording 4	98.13	39.99	1.87
Average	91.21	33.89	8.79

3.3.3 Comparison of Detection Modes

Five different modes of detection were compared namely, manual detection by inexperienced scorer on FIR filtered recordings (FIR/inexp), manual detection by experienced scorer on DWT denoised recordings (DWT/manual), automatic detection on FIR filtered recordings (FIR/auto), automatic detection on DWT denoised recordings (DWT/auto) and automatic detection on SWT denoised recordings (SWT/auto). The values of sensitivity for all four ENG recordings under the detection modes discussed above are given in the form of a table in table 3.22 and are plotted as a graph in figure 3.28. Figure 3.29 shows the error percentage of detection modes across all 4 recordings.

Table 3.22: Comparison of the sensitivity of five detection modes

Recording	Sensitivity (S)%				
	FIR/inexp	FIR/auto	DWT/manual	DWT/auto	SWT/auto
Recording 1	65.78	57.46	84.89	100	93.87
Recording 2	16.73	90.58	69.81	100	94.04
Recording 3	51.11	58.58	52.87	88.56	78.81
Recording 4	68.91	63.23	62.1	99.6	98.13
Average	50.63	67.46	67.42	97.04	91.21

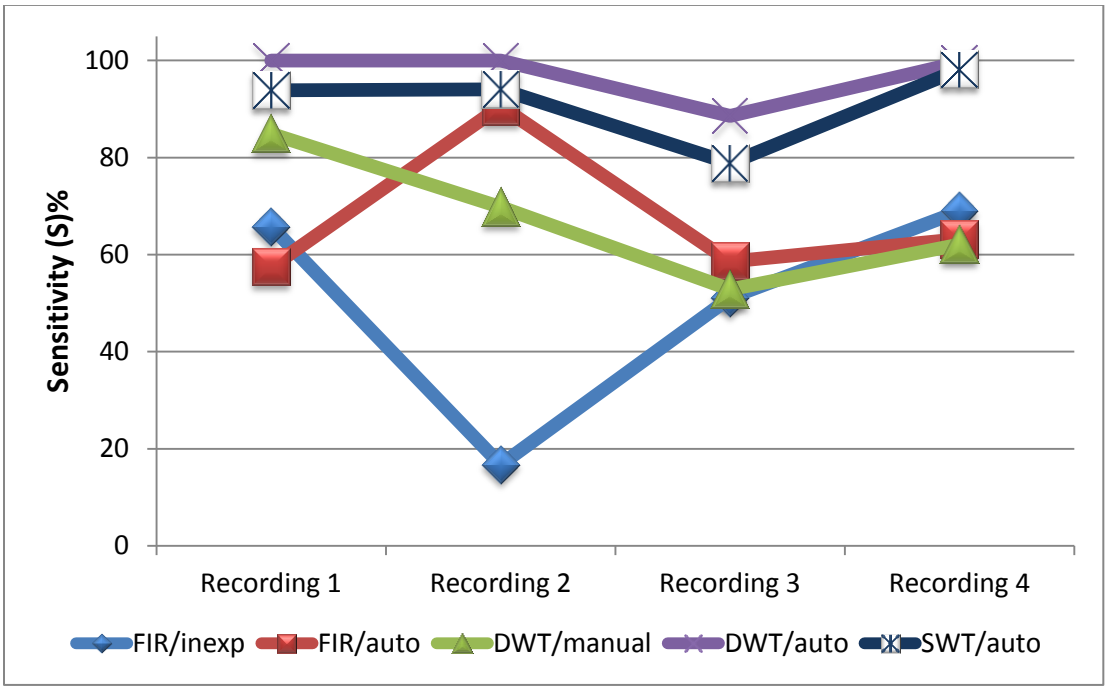

Figure 3.28: Graphical comparison of sensitivity of various detection modes on real ENG recordings

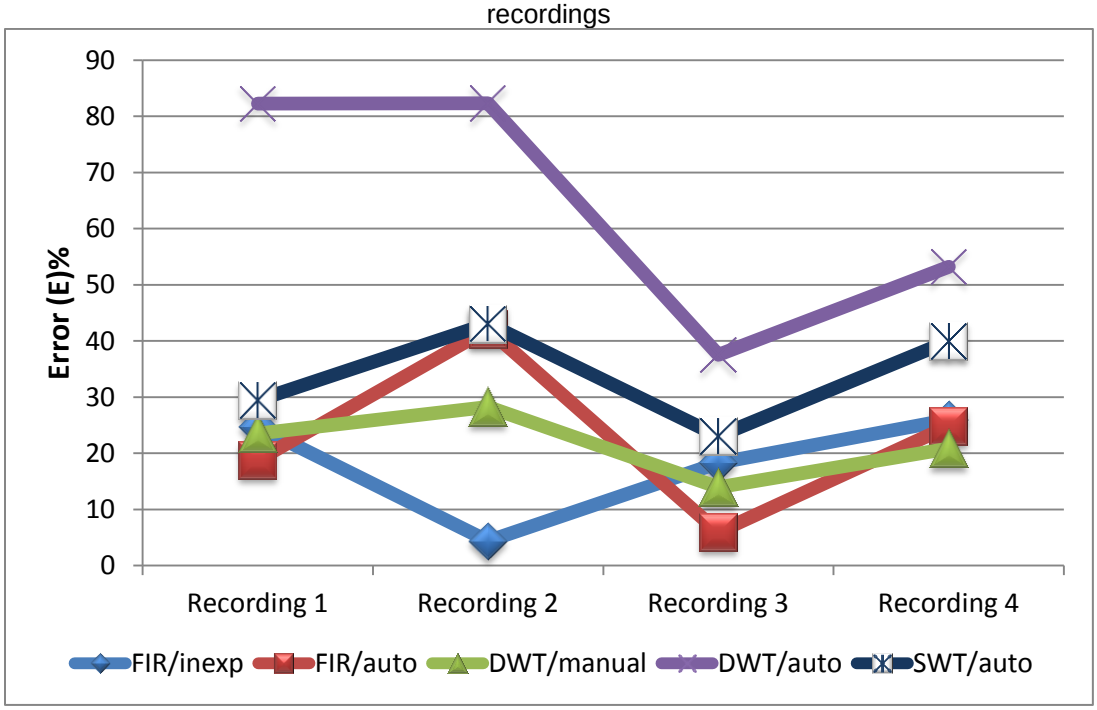

Figure 3.29: Graphical comparison of error of various detection modes on real ENG recordings

Statistical comparison between the five different modes of detection by the use of one-way ANOVA and the resulting p-value table is given in table 3.23. Since for both sensitivity and error, the results were significant, post-hoc analysis was performed using tukey's HSD test and the means were compared pair wise and the significance of the difference is noted in tables 3.24 and 3.25.

Table 3.23: ANOVA results for comparison of parameters between five detection modes used. Significant p-values are marked with an asterisk next to them.

Parameter compared	**p-value for one-way ANOVA**
Sensitivity (S)	0.0028*
Error (E)	0.0017*

Table 3.24: Pair wise comparison using Tukey's post-hoc test for Sensitivity (S) (NS: Not Significant)

	FIR/inexp	**FIR/auto**	**DWT/manual**	**DWT/auto**
FIR/inexp	-			
FIR/auto	NS	-		
DWT/manual	NS	NS	-	
DWT/auto	Significant	Significant	Significant	-
SWT/auto	Significant	Significant	Significant	NS

Table 3.25: Pair wise comparison using Tukey's post-hoc test for Error (E) (NS: Not Significant)

	FIR/inexp	**FIR/auto**	**DWT/manual**	**DWT/auto**
FIR/inexp	-			
FIR/auto	NS	-		
DWT/manual	NS	NS	-	
DWT/auto	Significant	Significant	Significant	-
SWT/auto	NS	NS	NS	Significant

Table 3.26: Comparison summary between the detection modes studied for real ENG recordings including the comparison of average processing time using MATLAB. TM denotes time taken for manual detection. Processing times are time taken per channel.

Detection Mode	Average computation time	Average Sensitivity (%)	Average Error (%)	Average Missed (%)
FIR/Inexp	2.4 s + TM	50.63	18.34	49.37
FIR/Auto	32.6 s	67.46	22.92	32.54
DWT/Manual	4.7 s + TM	67.42	21.66	32.58
DWT/Auto	34.3 s	97.04	63.82	2.96
SWT/Auto	56.6 s	91.21	33.89	8.79

A comparison summary between all the five detection modes tested comparing their average sensitivity, error and missed percentages along with the processing time is given in table 3.14. The processing times provided were the time taken per channel with the average length of a signal being 238 seconds (Approximately 4 minutes). The computer which was used to compute the processing times had an Intel Xeon Quad Core processor with 8 GB RAM and 2 GHz clock frequency running on Windows XP operating system.

CHAPTER 4

DISCUSSION AND CONCLUSION

In this chapter the results and findings of this study will be discussed with respect to the objectives stated in chapter 1 section 1.4.

4.1 Choice of Wavelet and Level of Decomposition for Wavelet Denoising

The first objective of this research was to compare the various wavelets and levels of decomposition suggested from literature. For this purpose, their performances in noise reduction, sensitivity of detection and detection error were compared. Table 3.2 shows standard deviation values for DWT denoised signals as percentages of standard deviation of the original signal (before it being denoised) for all 5 wavelets under both level 4 and level 5 decomposition. From this table and figure 3.1, which shows comparison between different wavelets at level 4 and level 5 DWT denoising, it can be concluded that the wavelets ‘haar’, ‘db4’ and ‘sym7’ reduce noise better than the wavelets ‘bior 3.5’ and ‘bior 3.7’ for level 4 DWT decomposition. Furthermore from figure 3.1, it can be inferred that the same conclusion holds for level 5 also.

Figure 3.2, shows the comparison between level 4 and level 5 DWT denoising, from which it can be inferred that level 5 denoising performs better than level 4 denoising in reducing the noise level of the signal and this is confirmed by the p-value of the t-test performed (p-value = 0.023). From the results discussed above, it is clear that DWT denoising at level 5 using the wavelets ‘haar’, ‘db4’ and ‘sym7’ perform better than all other combinations in terms of noise reduction.

The effect of the choice of wavelet as well as the level of decomposition on the sensitivity of detection of action potentials was examined for manual detection using DWT denoised signals, automatic detection using DWT and SWT denoised signals. For manual detection using DWT denoised simulated ENG signals. Referring to the results shown in table

3.7 and the figures 3.13 and 3.14, the sensitivity and detection error is most optimal for level 5 decomposition using ‘sym7’ wavelet and closely followed by level 5 decomposition using ‘haar’ wavelet.

For Automatic detection on DWT denoised signals, from the results shown in table 3.9 and from figures 3.16 and 3.17, level 5 decomposition using ‘sym7’ wavelet produces better results than all other combinations closely followed by level 4 decomposition using ‘sym7’ wavelet. The same holds true for automatic detection on SWT denoised signals from the results shown in table 3.10 and figures 3.18 and 3.19.

It is to be noted that the use of ‘haar’ wavelet only determines the presence or absence of an action potential and does not preserve the shape of an action potential unlike all other wavelets examined. However, when ‘haar’ wavelet is used, automatic detection algorithm stops at threshold detection hence making the process faster and robust. Therefore, for the purposes of determining just the ‘quantity’ of action potentials, ‘haar’ wavelet would be a good choice while its use would preclude any possible investigation of changes in its morphology and possible significance of such changes. Hence by examining the effect of the choice of wavelet and level of decomposition across all detection modes, level 5 decomposition using ‘symlet 7’ wavelet appears to perform the best, as this combination provided the best results consistently across all detection modes and noise levels.

4.2 Noise Reduction

The second objective of this study was to compare the performance of wavelet denoising to that of linear filtering that is now in use. For this purpose, the reduction of noise after wavelet denoising of both simulated ENG signals and real ENG recordings using FIR filtering, DWT denoising and SWT denoising were compared. From the statistical comparison (section 3.1.13) between FIR filtering, level 4 and level 5 DWT denoising, it can be concluded that level 4 DWT and level 5 DWT reduce noise significantly greater than FIR filtering (p-value = 0.0009).

The levels of noise reduction in real ENG recordings using FIR filtering, DWT and SWT denoising were compared. From table 3.4 and figure 3.3, it can be concluded that DWT and SWT denoising reduce noise better than FIR filtering. Statistical comparison using ANOVA (p-value = 3.11 E-06) and the resulting post-hoc test shows that both DWT and SWT reduce noise significantly more than FIR filtering. However, there is no significant difference between DWT and SWT denoising in terms of noise reduction.

4.3 Detection of Action Potentials in Simulated ENG Signals

4.3.1 Comparison of Detection Modes

Five detection modes were compared and from the results presented in table 3.11, figure 3.20 which shows the graphical comparison of sensitivities of detection and figure 3.21 which shows the average sensitivity and detection error of the five detection modes compared. Comparison was made between manual and automatic detection on FIR filtered and DWT denoised signals and the results of t-tests are provided in table 3.12. As is evident from the p-values given, automatic detection on FIR filtered signals produced significantly better sensitivity (p-value = 0.0045) and significantly less detection error (p-value = 0.0203) than manual detection on FIR filtered signals whereas the difference in DWT signals was statistically insignificant. One possible explanation for this is that the template was based on FIR filtered signals therefore causing the algorithm to perform better on FIR filtered signals than on DWT denoised signals.

Sensitivity and detection error was compared between different types of denoising and the results are shown in table 3.13. It can be seen that according to the statistical analysis , while automatic detection on FIR filtered signals produced significantly better sensitivity (p = 0.0036), it also had significantly greater detection error (p = 0.0240) than automatic detection on DWT denoised signals. Also, while the difference in sensitivities of detection between automatic detection using FIR filtered signals and automatic detection using SWT signals was not significant, the latter did have significantly lower detection error (p = 0.0114). Upon considering

both parameters, it can be concluded that automatic detection on SWT denoised signals performed better than all other detection modes.

4.4 Detection of Action Potentials in Real ENG Recordings

For the detection of action potentials in real ENG recordings, the performance of the experienced scorer on FIR filtered recordings was considered as the gold standard and all other detection modes were compared against this to determine sensitivity and error of detection.

4.4.1 Selection of Correlation Threshold for Automatic Detection of Action Potentials

The effect of correlation threshold value for automatic detection of action potentials was found to vary for each type of denoising employed. Hence, the results for sensitivity of detection across various correlation thresholds examined were presented for each detection mode. The results for automatic detection on FIR filtered recordings were presented in Figure 3.22 and it was concluded from the figure and the average sensitivity values that correlation threshold of C = 0.35 was the optimal value.

For automatic detection on DWT recordings, the results for various correlation thresholds were presented in figure 3.24 and upon examining the figure and the average values, the correlation threshold value of C = 0.50 was chosen to be the optimal value for this detection mode since this threshold value produced consistent sensitivity across all four recordings despite slightly increased error. A similar analysis for selection of correlation threshold value for automatic detection on SWT denoised recordings based on figure 3.26 and their average accuracy values, the optimal correlation threshold was chosen to be C = 0.50. The values at these thresholds were chosen for the purpose of performance comparison of all detection modes. One possible explanation for the differing thresholds is the difference in shape of action potentials after different types of denoising and hence would result in varying degrees of matching for a given correlation threshold using a set template.

4.4.2 Comparison of Detection Modes

The sensitivity and detection error of the various detection modes studied were compared across all 4 recordings and the results are shown in table 3.22 and in figures 3.28 and 3.29. From figures 3.28 and 3.29, it can be observed that while both automatic detection on DWT recordings and automatic detection on SWT recordings have high sensitivities, the detection error of automatic detection in DWT recordings is much greater than other detection modes. This can be verified with the help of Tukey's HSD post-hoc test on sensitivity and detection error, which are given in tables 3.24 and 3.25. It can be seen from the tables that while automatic detection on both DWT and SWT recordings have significantly greater sensitivities than other detection modes, automatic detection on DWT recordings also has significantly greater detection error than all other modes while there is no significant difference in detection error between automatic detection on SWT recordings and all other detection modes except for automatic detection on DWT recordings.

An explanation for greater detection error in automatic detection across all 3 denoising methods is the presence of action potentials in differing shapes that doesn't match as well with the template hence resulting in the need to lower the correlation threshold which causes the detection error to increase. A way to overcome this would be to add all known shapes of action potentials to the template database which would also enable the classification of action potentials by shape (by comparing a suspected action potential with all the templates and classifying it according to the highest correlation value). A possible explanation for lower accuracy in manual detection on DWT denoised signals is difference in the shape of action potentials in DWT denoised recordings when compared with FIR filtered recordings, to which they are accustomed to. It is to be noted that all denoising techniques alter the shape of a noisy signal such as an ENG to a certain extent (including FIR filtering) and the same shape would look slightly different under different denoising methods.

From the tables 3.14 and 3.26 which provide comparison of detection modes for simulated and real ENG recordings respectively, it can be concluded that among the different denoising methods compared, SWT denoising had the highest processing time for both simulated and real ENG recordings as well having the highest average sensitivity for automated detection on simulated signals. It should be noted that the processing times were for programs implemented using MATLAB and therefore should only be considered for comparison purposes as these times could be vastly reduced if the same programs were to be implemented using C++ or embedded C. A research done in California Polytechnic State University shows that the processing times could be decreased by a factor of 500 when programs are implemented in C++ rather than MATLAB (Andrews, 2012). Therefore, because of the high sensitivity and less error rate among all detection modes tested, automatic detection on SWT denoised signals could be considered the most effective.

4.5 Conclusion

It can be observed from the results and discussions provided in chapters 3 and 4 that wavelet denoising of ENG recordings reduce the noise significantly better than FIR filtering (p-value = 3.11 E-06) thereby enabling the detection of action potentials which may be buried in noise otherwise. From the results of simulated ENG signals, it is clear that automatic detection on SWT denoised signals provided the optimal combination of sensitivity and detection error than all other detection modes that were compared. Furthermore, automatic detection on FIR filtered signals proved to be significantly more sensitive than manual detection on FIR filtered signals (p-value = 0.0045). From the analysis on the results of real ENG recordings, automatic detection on SWT signals again produced the optimal combination of sensitivity and detection error than all other detection modes compared. Among all combinations of level of decomposition and wavelet compared, level 5 decomposition with ‘symlet 7’ wavelet consistently provided the most optimal results across all detection modes including manual detection.

4.6 Limitations and Future Work

The processing time for SWT denoising was comparatively higher than both FIR filtering and DWT denoising and as noted in section 4.4, this is mainly due to restrictions in MATLAB. Therefore, the programs could be implemented in either C++ or embedded C which would not only reduce the processing time but will also enable real time implementation for prosthetic control. One of the limitations was that the template was constructed from a very limited number of shapes of action potentials and did not account for all known shapes of action potentials therefore it may have adversely affected the performance of automatic detection. So the addition of all known shapes of action potentials to the template database could not only improve the performance of automatic detection, it could also enable the classification and sorting of action potentials which would in turn be used to differentiate action potentials originating from different axons near the electrode. The processing time for automatic detection could also be reduced by modifying the program by implementing memory allocation techniques in embedded C for real time implementation. Also, provision could be made to add new shapes to template database in real time. Another limitation of this study was that manual detection on SWT denoised signals was not performed due to unavailability of the expert scorer.

APPENDIX A

MATLAB PROGRAM FOR NOISE ANALYSIS

```
[fname, pathname] = uigetfile('.plx','select a plx file to read
from','MultiSelect','on');

for h = 1:5
    filename = fullfile(pathname, fname{h});

      for  k = 16:31
          channel = k;
          [adfreq, n, ts, fn, ad] = plx_ad_v(filename, channel);
          z = ad;
          std_raw = std(z)*1000;
          arr_std = num2cell(std_raw);

          %% WRITING TO EXCEL FILE

          fnm = ('G:\mani\denoising real files for analysis\noise
          analysis\dwt_noise.xlsx');
          [num,txt,raw] = xlsread(fnm);
          S = size(raw);
          starting_line = S(1) + 1;
          newraw = cell(S(1)+2,S(2));
          for i = 1:S(1)
              newraw(i,:) = raw(i,:);
          end

          if k == 16
            newraw(starting_line,1) = cellstr(fname{h});
            newraw(starting_line+1,1) = strcat({'Channel'},{'
            '},cellstr(num2str(k)));
            newraw(starting_line+1,2) = arr_std;
          else
            newraw(starting_line,1) = strcat({'Channel'},{'
            '},cellstr(num2str(k)));
            newraw(starting_line,2) = arr_std;
          end
          xlswrite(fnm,newraw);

      end
      disp(strcat('finished file :',int2str(h)));
end

    fprintf(1,'\n  The above results have been added to the file
%s.\n\n\n', fnm);
```

APPENDIX B

MATLAB PROGRAM FOR GENERATING SIMULATED ENG SIGNALS

```
% PROGRAM TO GENERATE SIMULATED ENG SIGNALS AND ADD WHITE GAUSSIAN
NOISE TO THEM

%% Initializing variables

fs = 40000;
count = 0;
current = 0;
current1 = 0;
current2 = 0;
current3 = 0;
vf = 0;

%% Generating Simulated signal

for i = 1:275
    sz1 = 200+round(rand*4000); % 200 = dead time
    sz2 = 200+round(rand*4000);
    sz3 = 200+round(rand*4000);
    r1 = round(rand*1800); % 1800 = size of the matrix actions 1 to
pick a random action potential from it.
    v1 = zeros(1,sz1);
    v2 = actions(r1+1,:);
    wf1_samp = length(vf) + sz1;
    wf1_ts = wf1_samp/fs; % to find the time stamp.
    v3 = zeros(1,sz2);
    r2 = round(rand*1800);
    v4 = (actions(r2+4,:)*0.66);
    wf2_samp = length(vf) + sz1 + sz2 + 56;
    wf2_ts = wf2_samp/fs;
    v5 = zeros(1,sz3);
    r3 = round(rand*1800);
    v6 = (actions(r3+4,:)*0.33);
    wf3_samp = length(vf) + sz1 +sz2 + sz3 + 112;
    wf3_ts = wf3_samp/fs;
    vf = [ current horzcat(v1,v2,v3,v4,v5,v6)];
    waveform1_timestamps = [current1 wf1_ts];
    waveform2_timestamps = [current2 wf2_ts];
    waveform3_timestamps = [current3 wf3_ts];
    current = vf;
    current1 = waveform1_timestamps;
    current2 = waveform2_timestamps;
    current3 = waveform3_timestamps;
    count = count + 1;
end

waveform1_timestamps =
waveform1_timestamps(2:length(waveform1_timestamps));
waveform2_timestamps =
waveform2_timestamps(2:length(waveform2_timestamps));
waveform3_timestamps =
waveform3_timestamps(2:length(waveform3_timestamps));
```

```
%% plotting the simulated signal

total_time = length(vf)/fs;
t = 0:(1/fs): total_time ;
l_t = length(t);
figure;
plot(t(2:l_t),vf);
xlabel('Time(Seconds)');
ylabel('Voltage(mV)');
hold on
plot(t(2:l_t),y);

%% adding noise to the simulated signal

snr = 0;
y = awgn(vf,snr,'measured');
std_sim = std(y);
figure;
plot(t(2:400000),vf(2:400000),'g');
xlabel('Time (S)');
ylabel('Voltage (µV)');
hold on
plot(t(2:400000),y(2:400000));
figure;
plot(t(2:l_t),vf);
xlabel('Time (S)');
ylabel('Voltage (µV)');
figure;
plot(t(2:l_t),y);
xlabel('Time (S)');
ylabel('Voltage (µV)');
```

APPENDIX C

MATLAB PROGRAM FOR WAVELET DENOISING

```
% FUNCTION TO DENOISE SIGNALS USING STATIONARY WAVELET TRANSFROM.
% syntax : denoised = m_swt(original_signal,level,wavelet);
% output: denoised - signal after denoising (same length as input
vector)
% inputs: original_signal - signal vector that needs to be denoised
%         level           - level of decomposition
%         wavelet         - wavelet to be used.
% example : y_denoised = m_swt(y,5,'db4');

function [y] = m_swt(z,level,wavel)
      %% configuring z
      size_z = size(z);
      if(size_z(2) ~= 1)
          z = z';
      end

      %% the right size
      s = length(z);
      pow = 2^level;
      s_ok = 0;
      if rem(s,pow)>0
          s_ok = ceil(s/pow)*pow;
          diff = s_ok - s;
          z = vertcat(z,zeros(diff,1));
      end

      %% swt

      [ca,cd] = swt(z,level,wavel);

      for i = 1:level
          det = cd(i,:);
          sig = std(z);
          n = length(det);
          thr = sig*(0.3936+0.1829*log2(n));
          for j = 1:length(det)
              if abs(det(j)) < thr
                  det(j) = 0;
              end
          end
          cd(i,:) = det;
      end

      y = iswt(ca,cd,wavel);

      if s_ok > 0
          y = y(1:s);
          z = z(1:s);
      end
end
```

APPENDIX D

MATLAB PROGRAM FOR AUTOMATIC DETECTION

```
%FUNCTION TO AUTOMATICALLY DETECT ACTION POTENTIALS BASED ON A
TEMPLATE
% syntax: [result] = autodetect(filename,template);
% output: detected action potentials in a *.mat file in the same
directory as input file with an extension '_autodetected' to the input
filename.

function [result] = autodetect(filename,temp)
result = 0;

if (nargin == 0 || isempty(filename))
   [fname, pathname] = uigetfile('*.nex', 'Select a NeuroExplorer
file','Multiselect','On');
   if isequal(fname,0)
     error 'No file was selected'
   end
end

for l = 1:length(fname)
    filename = fullfile(pathname, fname{l});
    [nexFile] = readNexFile(filename);
    filename2 = strcat(filename(1:end-4),'_autodetected','.mat');
    file_ts = cell(16,1);
    file_wave = cell(16,1);
    file_cor = cell(16,1);

%% thresholding and detecting

for m = 1:16
    z = nexFile.contvars{m,1}.data;
    y = z';
    thr = -4*std(y);
    l_y = length(y) ;
    fs = 40000;
    total_time = l_y/fs;
    t = 0:(1/fs): total_time ;
    t = t(2:length(t));
    l_t = length(t);
    avoidable = 0;
    current1 = zeros(1,56);
    current2 = 0;
    current3 = 0;
    current4 = 0;
    current5 = zeros(1,56);

    for i = 50:(l_t-71)
        if y(i) <= thr
            if t(i) > avoidable
                waveform = y((i-15):(i+40))';
                max_amp_wave = max(waveform) - min(waveform);
                if max_amp_wave > 3*abs(thr)
```

```
                    wave = waveform';
                    [corr_value lags] = xcorr(temp,wave,'biased');
                    max_cv = max(corr_value);
                    ind = find(corr_value == max_cv);
                    lag_max_cv = lags(ind);
                    min_ind = i-15-lag_max_cv;
                    max_ind = i+40-lag_max_cv;
                    waveform = y(min_ind:max_ind);
                    cor = corr2(temp,waveform);
                    time = t(min_ind);
                    cor_matrix = [current3; cor];
                    waveform_matrix = [current1; waveform];
                    time_matrix = [current2; time];
                    current1 = waveform_matrix;
                    current2 = time_matrix;
                    current3 = cor_matrix;
                end
                avoidable = t(i+70);
            end
        end
    end
    siz_det = size(waveform_matrix);
    num_det = siz_det(1);
    waveform_matrix = waveform_matrix(2:num_det,1:56);
    time_matrix = time_matrix(2:length(time_matrix));
    cor_matrix = cor_matrix(2:length(cor_matrix));
    siz_det = size(waveform_matrix);
    num_det = siz_det(1);

    %% template correlation coefficient based detection

    for i = 1:num_det
        if cor_matrix(i) > 0.55
                ts = [current4 time_matrix(i)];
                wave_matrix = [current5 ; waveform_matrix(i,:)];
                current4 = ts;
                current5 = wave_matrix;
        end
    end
    if length(current4) > 1
        wave_matrix = wave_matrix(2:length(ts),:);
        ts = ts(2:length(ts));
    else
        wave_matrix = [];
        ts = [];
    end
    file_wave{m,1} = wave_matrix;
    file_ts{m,1} = ts;
    file_cor{m,1} = cor_matrix;
    disp(strcat('finished processing channel : ',int2str(m),' of
file:',int2str(l)));
end
```

```
save(filename2,'file_wave','file_ts','file_cor');
fprintf(1,'\n successfully written variables to file : %s \n',
filename2);
end
result = 1;
end
```

REFERENCES

[1] Adamos, D., E. Kosmidis, and G. Theophilidis. "Performance Evaluation of PCA-based Spike Sorting Algorithms." *Computer Methods and Programs in Biomedicine* 91.3 (2008): 232-44. Print.

[2] Akay, Metin, and Claudia Mello. "Wavelets for Biomedical Signal Processing." *Engineering in Medicine and Biology Society, 1997. Proceedings of the 19th Annual International Conference of the IEEE* 6 (1997): 2688-691. Print.

[3] Andrews, Tyler. "Computation Time Comparison Between Matlab and C++ Using Launch Windows." (2012).

[4] Atkins, Diane J., Denise C.Y. Heard, and William H. Donovan. "Epidemiologic Overview of Individuals with Upper-Limb Loss and Their Reported Research Priorities." *JPO Journal of Prosthetics and Orthotics* 8.1 (1996): 2. Print.

[5] Bernstein, J. "Ueber Den Zeitlichen Verlauf Der Negativen Schwankung Des Nervenstroms." *Pflüger, Archiv Für Die Gesammte Physiologie Des Menschen Und Der Thiere* 1.1 (1868): 173-207. Print.

[6] Biddiss, Elaine, and Tom Chau. "Upper Limb Prosthesis Use and Abandonment: A Survey of the Last 25 Years." *Prosthetics and Orthotics International* 31.3 (2007): 236-57. Print.

[7] Branner, Almut, and Richard Alan Normann. A Multielectrode Array for Intrafascicular Recording and Stimulation in Sciatic Nerve of Cats. *Brain Research Bulletin*, 51(4)(2000): 293-306.

[8] Brychta, Robert J., Richard Shiavi, David Robertson, and André Diedrich. "Spike Detection in Human Muscle Sympathetic Nerve Activity Using the Kurtosis of Stationary

Wavelet Transform Coefficients." *Journal of Neuroscience Methods* 160.2 (2007): 359-67. Print.Burch, George E., and Nicholas P. DePasquale. *A History of Electrocardiography*. Chicago: Year Book Medical, 1964. Print.

[9] Chervin, Ronald D., and Christian Guilleminault. "Diaphragm Pacing for Respiratory Insufficiency." *Journal of Clinical Neurophysiology* 14.5 (1997): 369-77. Print.

[10] Cho, Sung-Hoon, Hong Meng Lu, Lawrence Cauller, Mario I. Romero-Ortega, Jeong-Bong Lee, and Gareth A. Hughes. "Biocompatible SU-8-Based Microprobes for Recording Neural Spike Signals From Regenerated Peripheral Nerve Fibers." *IEEE Sensors Journal* 8.11 (2008): 1830-836. Print.

[11] Choi, J.H., H.K. Jung, and T. Kim. "A New Action Potential Detector Using the MTEO and Its Effects on Spike Sorting Systems at Low Signal-to-Noise Ratios." *IEEE Transactions on Biomedical Engineering* 53.4 (2006): 738-46. Print.

[12] Citi, Luca, Jacopo Carpaneto, Ken Yoshida, Klaus-Peter Hoffmann, Klaus Peter Koch, Paolo Dario, and Silvestro Micera. "On the Use of Wavelet Denoising and Spike Sorting Techniques to Process Electroneurographic Signals Recorded Using Intraneural Electrodes." *Journal of Neuroscience Methods* 172.2 (2008): 294-302. Print.

[13] Dakpa, R. "Prosthetic Management and Training of Adult Upper Limb Amputees." *Current Orthopaedics* 11.3 (1997): 193-202. Print.

[14] Daubechies, I. (1990). The Wavelet Transform, Time-frequency Localization and Signal Analysis. Information Theory, *IEEE Transactions On, 36*(5), 961-1005.

[15] Della Santina, C. C., Kovacs, G. T., & Lewis, E. R. (1997). Multi-unit Recording from Regenerated Bullfrog Eighth Nerve Using Implantable Silicon-substrate Microelectrodes. *Journal of Neuroscience Methods*, 72(1), 71.

[16] Diedrich, A., W. Charoensuk, R.J. Brychta, A.C. Ertl, and R. Shiavi. "Analysis of Raw Microneurographic Recordings Based on Wavelet De-noising Technique and

Classification Algorithm: Wavelet Analysis in Microneurography." *IEEE Transactions on Biomedical Engineering* 50.1 (2003): 41-50. Print.

[17] Donoho, D. L. (1995). De-noising by Soft-thresholding. *Information Theory, IEEE Transactions On* , 41(3), 613-627.

[18] Freeman, Scott, and Healy Hamilton. *Biological Science*. 2nd ed. Upper Saddle River, NJ: Pearson Prentice Hall, 2005. Print.

[19] Garde, K., Keefer, E., Botterman, B., Galvan, P., & Romero, M. I. (2009). Early Interfaced Neural Activity from Chronic Amputated Nerves. *Frontiers in Neuroengineering*, *2*.

[20] Hagbarth, Karl-Erik. "Microelectrode Recordings from Human Peripheral Nerves (microneurography)." *Muscle & Nerve* 25.S11 (2002): S28-35. Print.

[21] Hulata, E., Segev, R., & Ben-Jacob, E. (2002). A Method for Spike Sorting and Detection Based on Wavelet Packets and Shannon's Mutual Information. *Journal of Neuroscience Methods, 117*(1), 1-12.

[22] Jia, X., M. Koenig, X. Zhang, J. Zhang, T. Chen, and Z. Chen. "Residual Motor Signal in Long-Term Human Severed Peripheral Nerves and Feasibility of Neural Signal-Controlled Artificial Limb." *The Journal of Hand Surgery* 32.5 (2007): 657-66. Print.

[23] Jiang, Youxing, et al. "X-ray structure of a voltage-dependent K+ channel."*Nature* 423.6935 (2003): 33-41.

[24] Kamavuako, Ernest Nlandu, Winnie Jensen, Ken Yoshida, Mathijs Kurstjens, and Dario Farina. "A Criterion for Signal-based Selection of Wavelets for Denoising Intrafascicular Nerve Recordings." *Journal of Neuroscience Methods* 186.2 (2010): 274-80. Print.

[25] Kim, K. H., & Kim, S. J. (2000). Neural Spike Sorting under Nearly 0-dB Signal-to-noise Ratio Using Nonlinear Energy Operator and Artificial Neural-network Classifier. *Biomedical Engineering, IEEE Transactions On, 47*(10), 1406-1411.

[26] Korivi, Naga S., and Pratul K. Ajmera. "Clip-on Micro-cuff Electrode for Neural Stimulation and Recording." *Sensors and Actuators B: Chemical* 160.1 (2011): 1514-519. Print.

[27] Kovacs, G. T., Storment, C. W., & Rosen, J. M. (1992). Regeneration Microelectrode Array for Peripheral Nerve Recording and Stimulation. Biomedical Engineering, IEEE Transactions On, 39(9), 893-902.

[28] Mallat, S. G. (1989). A Theory for Multiresolution Signal Decomposition: the Wavelet Representation. Pattern Analysis and Machine Intelligence, *IEEE Transactions On, 11*(7), 674-693.

[29] Mannard, A., R. B. Stein, and D. Charles. "Regeneration Electrode Units: Implants for Recording from Single Peripheral Nerve Fibers in Freely Moving Animals." *Science* 183.4124 (1974): 547-49. Print.

[30] "Microsystems Lab (University of Utah)." *Microsystems Lab (University of Utah)*. N.p., n.d. Web. 08 Nov. 2012. <http://www.microsystems.utah.edu/inip>.

[31] Navarro, X., Calvet, S., Butí, M., Gómez, N., Cabruja, E., Garrido, P., & Valderrama, E. (1996). Peripheral Nerve Regeneration through Microelectrode Arrays Based on Silicon Technology. Restorative Neurology and Neuroscience, 9(3), 151-160.

[32] Navarro, X., Calvet, S., Rodriguez, F. J., Stieglitz, T., Blau, C., Buti, M., & Meyer, J. U. (1998). Stimulation and Recording from Regenerated Peripheral Nerves through Polyimide Sieve Electrodes. *Journal of the Peripheral Nervous System: JPNS*, 3(2), 91.

[33] Navarro, Xavier, Thilo B. Krueger, Natalia Lago, Silvestro Micera, Thomas Stieglitz, and Paolo Dario. "A Critical Review of Interfaces with the Peripheral Nervous System for the Control of Neuroprostheses and Hybrid Bionic Systems." *Journal of the Peripheral Nervous System* 10.3 (2005): 229-58. Print.

[34] O'Doherty, Joseph E., Mikhail A. Lebedev, Peter J. Ifft, Katie Z. Zhuang, Solaiman Shokur, Hannes Bleuler, and Miguel A. L. Nicolelis. "Active Tactile Exploration Using a Brain–machine–brain Interface." *Nature* 479.7372 (2011): 228-31. Print.

[35] Oweiss, K. G., & Anderson, D. J. (2002). Spike Sorting: a Novel Shift and Amplitude Invariant Technique. *Neurocomputing, 44*, 1133-1139.

[36] Piccolino, M. "Animal Electricity and the Birth of Electrophysiology: The Legacy of Luigi Galvani." *Brain Research Bulletin* 46.5 (1998): 381-407. Print.

[37] Resnik, Linda, Marissa R. Meucci, Shana Lieberman-Klinger, Christopher Fantini, Debra L. Kelty, Roxanne Disla, and Nicole Sasson. "Advanced Upper Limb Prosthetic Devices: Implications for Upper Limb Prosthetic Rehabilitation." *Archives of Physical Medicine and Rehabilitation* 93.4 (2012): 710-17. Print.

[38] Rossini, Paolo M., Silvestro Micera, Antonella Benvenuto, Jacopo Carpaneto, Giuseppe Cavallo, Luca Citi, Christian Cipriani, Luca Denaro, Vincenzo Denaro, and Giovanni Di Pino. "Double Nerve Intraneural Interface Implant on a Human Amputee for Robotic Hand Control." *Clinical Neurophysiology* 121.5 (2010): 777-83. Print.

[39] Sanderson, J. Burdon, and F. J. M. Page. "Experimental Results Relating to the Rhythmical and Excitatory Motions of the Ventricle of the Heart of the Frog, and of the Electrical Phenomena Which Accompany Them." *Proceedings of the Royal Society of London (1854-1905)* 27 (1878): 410-14. Print.

[40] Sato, Chikara, et al. "The voltage-sensitive sodium channel is a bell-shaped molecule with several cavities." *Nature* 409.6823 (2001): 1047-1051.

[41] Schuetze, Stephen M. "The Discovery of the Action Potential." *Trends in Neurosciences* 6 (1983): 164-68. Print.

[42] Seifert, J. L., Desai, V., Watson, R. C., Musa, T., Kim, Y. T., Keefer, E. W., & Romero, M. I. (2012). Normal Molecular Repair Mechanisms in Regenerative Peripheral Nerve

Interfaces Allow Recording of Early Spike Activity Despite Immature Myelination. *Neural Systems and Rehabilitation Engineering, IEEE Transactions On*, 20(2), 220-227.

[43] Stein, R., and V. Mushahwar. "Reanimating Limbs after Injury or Disease." *Trends in Neurosciences* 28.10 (2005): 518-24. Print.

[44] Strege, D., W. Cooney, M. Wood, S. Johnson, and B. Metcalf. "Chronic Peripheral Nerve Pain Treated with Direct Electrical Nerve Stimulation☆." *The Journal of Hand Surgery* 19.6 (1994): 931-39. Print.

[45] Thakur, Pramodsingh H., et al. "Automated optimal detection and classification of neural action potentials in extra-cellular recordings." *Journal of Neuroscience Methods* 162.1 (2007): 364-376.

[46] Torebjörk, H. E., A. B. Vallbo, and J. L. Ochoa. "Intraneural Microstimulation in Man Its Relation to Specificity of Tactile Sensations." *Brain* 110.6 (1987): 1509-529. Print.

[47] Tyler, Dustin J., and Dominique M. Durand. "A Slowly Penetrating Interfascicular Nerve Electrode for Selective Activation of Peripheral Nerves." *Rehabilitation Engineering, IEEE Transactions on* 5.1 (1997): 51-61. Print.

[48] Vargas-Irwin, Carlos, and John P. Donoghue. "Automated Spike Sorting Using Density Grid Contour Clustering and Subtractive Waveform Decomposition." *Journal of Neuroscience Methods* 164.1 (2007): 1-18. Print.

[49] Velliste, Meel, Sagi Perel, M. Chance Spalding, Andrew S. Whitford, and Andrew B. Schwartz. "Cortical Control of a Prosthetic Arm for Self-feeding." *Nature* 453.7198 (2008): 1098-101. Print.

[50] Vogelstein, R. J., Murari, K., Thakur, P. H., Diehl, C., Chakrabartty, S., & Cauwenberghs, G. (2004, September). Spike Sorting with Support Vector Machines. *In Engineering in Medicine and Biology Society, 2004. IEMBS'04. 26th Annual International Conference of the IEEE* (Vol. 1, Pp. 546-549). IEEE.

[51] Wiltschko, A., G. Gage, and J. Berke. "Wavelet Filtering before Spike Detection Preserves Waveform Shape and Enhances Single-unit Discrimination." *Journal of Neuroscience Methods* 173.1 (2008): 34-40. Print.

[52] Yoshida, Ken, and Richard B. Stein. "Characterization of Signals and Noise Rejection with Bipolar Longitudinal Intrafascicular Electrodes." *Biomedical Engineering, IEEE Transactions on* 46.2 (1999): 226-34. Print.

[53] Zhang, Q., Y. Liu, L. Brown, and J. Shoemaker. "Challenges and Opportunities in Processing Muscle Sympathetic Nerve Activity with Wavelet Denoising Techniques: Detecting Single Action Potentials in Multiunit Sympathetic Nerve Recordings in Humans." *Autonomic Neuroscience* 134.1-2 (2007): 92-105. Print.

BIOGRAPHICAL INFORMATION

Manikandan Ravi was born in the 2nd of June, 1989 in a small town called Rajapalayam near Madurai, India. His parents decided to give him better education and moved him to the capital city of Chennai where he was educated from 6th grade onwards. He decided to pursue a bachelor's degree in biomedical engineering from Jerusalem College of Engineering, Anna University and graduated first class in 2010. His final year project was on building a smart alarm clock using EEG signals on which he has co-authored a paper published in IJBET. Soon after graduating, he decided to pursue M.S in Bioengineering from University of Texas at Arlington. At UTA, he was involved in a project to effectively denoise ENG signals using wavelet transform and automatically detect action potentials from them. His research interests include biomedical signal processing and biomedical instrumentation.